

Abstract

The author, as a meteorological research member of the Wintering Party of the Eleventh Japanese Antarctic Research Expedition in 1969–1971, carried out micro-meteorological observations at Syowa Station in Antarctica during the period from February 1970 to February 1971. The results have been reported in the following papers: MAKI (1971); MAKI (1972a, b, c, d); and MAKI (1974a, b).

The observations on the structure of the atmospheric turbulence near the ground were made with the sonic anemometer-thermometer for the first time as the main theme of the meteorological research project. This investigation was carried out for the first year in the four year project of "Explanation of Formation and Structure of Antarctic Anticyclone".

An atmospheric turbulence in stable stratification was measured on the 21 m-high tower built on the sloping terrain of Syowa Station during the period from February to December, 1970. Its characteristics are analyzed in relation to the stability (Richardson number, Ri) in the atmospheric surface layer.

The vertical mean wind speed at the height of 20 m is observed to be about one-third of the longitudinal mean wind speed at the same height (U_{20}) above the slope with the inclination of about 10 degrees. The standard deviations of the longitudinal, lateral and vertical wind speed fluctuations decrease exponentially with the increase of Ri . The ratios of the standard deviations of the longitudinal, lateral and vertical wind speed fluctuations to the friction velocity are independent of Ri . The energy dissipation rate increases roughly in proportion to the 0.5 power of Ri . The scale of the atmospheric turbulence seems to be a solid body of a long and narrow cubic vortex having the dimensions of length : breadth : height = 6.3 : 1.9 : 1. The characteristic scale of the atmospheric turbulence which is the largest turbulon (INOUE *et al.*, 1955) is independent of the stability (Ri). Furthermore, the scale of the smallest turbulon increases exponentially with the value of Ri . The nondimensional frequency at the maximum spectral density of the longitudinal wind speed increases with the increase of Ri . On the other hand, the peak frequency of the lateral wind speed is independent of Ri , and that of the vertical wind speed decreases with the increase of Ri .

The interrelations among the wind direction, the wind velocity, the air tempera-

ture and the vertical air temperature gradient have become clear as follows: In winter, the frequency of the prevailing wind direction is not higher than that in other seasons. The frequencies of the southern wind directions of S and SSE, the frequency of the dead calm (below 0.1 m/s) and the wind speed of the prevailing wind in winter are higher than those in other seasons. The air temperatures are high in the wind directions of NNE to E, and low in the wind directions of SSW and SW. The vertical air temperature gradient in stable stratification is large in the wind directions of ESE to SSW and decreases rapidly with the increase of the wind velocity below about 10 m/s and gently above about 10 m/s.

The warming ratio which is defined as the ratio of the increase of air temperature to the increase of wind velocity shows a significant annual variation. The warming ratio is 2.9°C per 10 m/s in spring, 1.3°C in summer, 3.0°C in autumn and 5.0°C in winter, particularly 5.8°C in May and August and 0.5°C in December. The vertical air temperature gradient decreases 0.0057°C/m with the 1°C increase of air temperature. The frequency of stable condition is about 88% in winter, about 30% in summer and about 75% throughout the year. The maximum of the frequency distribution of the vertical air temperature gradient shifts from the maximum of the normal distribution to the unstable side in winter, and *vice versa* in summer. The Kernlose-type phenomenon also appears in the annual variations of the tropospheric maximum air temperature and of the air temperature at the heights of 20 m and 1 m. The meteorological observations made on the tower on the sloping terrain of Syowa Station may not be ideal as a representative meteorological observation in Antarctica.

The observation of the atmospheric surface layer in super-stable stratification was carried out in the middle of the Ongul Strait about 2 km east of Syowa Station. The author obtained the relations of the stability ratio (S) to the momentum diffusion coefficient, to the mixing length, and to the Richardson number against heights in strong stable stratification. The vertical profile of air temperature shows a perfect linear variation in winter and a nearly linear variation in spring. The relation between the vertical air temperature gradient and the wind velocity at the height of 6 m (U_6) is similar to an orthogonal hyperbola above 2.0 m/s of U_6 .

The author also investigated the relation between the visibility and the wind velocity under the condition of drifting snow. The visibility decreases rapidly with the increase of the wind velocity at the height of 10 m (U_{10}) above 8 m/s, namely, when U_{10} is 15 m/s the visibility is about 150 m; 25 m/s, 10 m; and 35 m/s, 2–3 m. The visibility is in inverse proportion to the fifth power of the wind velocity. The deduction of different friction drags obtained under constant or changeable aerodynamic roughness lengths is almost proportional to the fifth power of the wind velocity and is almost inversely proportional to the visibility.

The turbulent heat transfer was measured on the smooth terrain at about 150 m north of the Air-Traffic Control Hut. The values obtained by two different methods of calculation of the turbulent heat flux agree considerably, when the sun rises scarcely above the horizon.

1. Introduction

The atmospheric turbulence in stable stratification was observed at Syowa Station (69°00'S, 39°35'E) in Antarctica during the period from February to December, 1970. Turbulence characteristics are analyzed in relation to the stability (Richardson number, Ri) or the wind speed at the height of 20 m in the surface air layer.

A great number of investigations have been made on the structure of atmospheric turbulence, especially on power spectra of wind speeds in the surface air layer during the last decade: SHIOTANI (1963), LUMLEY and PANOFSKY (1964), SOMA (1964), BERMAN (1965), KAIMAL and IZUMI (1965), SAHASHI (1967), MITSUTA (1968a, b), BUSCH *et al.* (1968), BUSCH and PANOFSKY (1968), BUSINGER *et al.* (1969), OKAMOTO and WEBB (1970), MITSUTA *et al.* (1970), MIYAKE, DONELAN and MITSUTA (1970), MIYAKE and McBEAN (1970), MIYAKE, STEWART and BURLING (1970), SITARAMAN (1970), YOKOYAMA (1971), WARNER (1972) and KAIMAL *et al.* (1972).

Although the energy and mass exchanges between the air and the ice cap in the polar regions are well known to play an important role in polar climate, our knowledge of the structure of air flow over the snow and ice in Antarctica is insufficient for clarifying the physical processes governing the interaction between the air and the ice cap. Little investigation has been made on the turbulence structure in super stable stratification as observed in the polar regions, so far as the author knows.

Observations on the structure of the atmospheric turbulence near the ground in super-stable stratification were carried out with the sonic anemometer-thermometers (S.A.T. hereafter) at Syowa Station during the period from February to December, 1970.

Wind fluctuation data are mainly analyzed in order to clarify their statistical characteristics in relation to the thermal stratification.

The relations among the climatic elements were made clear by the observation during the period from March 1970 to February 1971 at Syowa Station. The past Wintering Party reported on the climatic elements such as wind direction, wind velocity and air temperature.

The climatic elements at Syowa Station have been already reported by some members of the Wintering Party. For example; annual wind rose, monthly mean wind direction, monthly mean wind velocity, monthly mean air temperature, annual frequency

of wind direction and annual frequencies of wind velocity for the wind direction and for the air temperature were reported by MURAKOSHI (1958), monthly mean wind velocity and wind rose by NAKASHIMA (1961), ten-day mean maximum and minimum temperatures by MURAKOSHI and YATA (1962), monthly wind rose, air temperature frequency for the wind direction in winter (June, July, August) and air temperature against the wind velocity in winter by Japan Meteorological Agency (1964) and annual wind velocity for the wind direction by MORITA (1968).

Accordingly, it is not so much original that similar variations of monthly and seasonal means of wind direction, wind velocity and air temperature are obtained. Therefore, the author made a study on annual variations of climatic elements consisting of monthly and seasonal variations. Especially, the vertical air temperature gradient (hereafter temperature gradient) is placed among the climatic elements along with the wind direction, the wind velocity and the air temperature. It was not reported in detail until now, particularly on the quantitative measurements of the increase of air temperature and the decrease of temperature gradient against the increase of wind velocity, and also the annual observation of the inversion layer and the relations among the temperature gradient and other climatic elements.

The author describes the characteristics of the wind velocity profile and the air temperature profile in the atmospheric surface layer, *i.e.*, annual occurrence ratio of ground inversion, air temperature difference of two different heights, altitude of tropospheric maximum air temperature and typical seasonal profile of air temperature.

The observations of the atmospheric surface layer in stable stratification above the sea ice are reported in the present paper. The author observed profiles of wind velocity, air temperature and snow temperature in the observation caboose during the period of one month when the annual minimum air temperature would appear frequently around Syowa Station.

The stability above the sea ice is generally larger than that at Syowa Station (MAKI, 1972a, b). Strong inversions with the temperature gradient of $2.0^{\circ}\text{C}/\text{m}$ were observed several times in the atmospheric surface layer above the sea ice. In such a strong stable stratification above the sea ice near Syowa Station, the usual equation of the wind velocity profile such as the logarithmic law is not applicable in the conditions of slightly stable to super-stable stratifications.

LILJEQUIST (1957) reports that a certain equation of the mixed form of the logarithmic and linear law is applicable to the strong stability from slightly stable to super-stable stratifications. The present results are compared after the method of LILJEQUIST (1957).

Now, the author reports the relation between the visibility and the wind velocity in drifting snow at Syowa Station. In Antarctica, the wind velocity is not strong without snow particles drifting from the surfaces of ice sheet and snow ice. In blizzard accompanied by the drifting snow and the snowfall, the visibility gets particularly poor and it is extremely dangerous for people to walk in the snow field. There has been no quantitative investigation of the relation between the wind velocity and the visibility except the work by LILJEQUIST (1957). The observation of visibility under

various wind velocities was carried out during the winter season from May to August, 1970.

Furthermore, the turbulent heat flux is obtained by two different methods, one of them calculates from the energy budget equation and the other from the functional formula including a wind component. The data for this research were obtained on the sea ice near Syowa Station during five days when the sun did not rise above the horizon.

If there is no short-wave radiation, the energy budget is represented by a very simple equation, as the former turbulent heat flux of two different methods is obtained from the net radiation and the vertical snow temperature profiles. On the other hand, the latter turbulent heat flux of two different methods is obtained from the vertical profiles of wind velocity and air temperature. The turbulent heat transfers obtained by two different methods are compared with each other.

2. Observations and Data Analyses

2.1. The observations were carried out at the micrometeorological observation site (point C in Fig. 1) of Syowa Station on East Ongul Island. The site slopes down eastward with the inclination of about 10 degrees. It is about 50 m away from the foot of the slope and about 30 m away from the snow line of the sea ice. The height of the site is about 8 m above the sea level. East Ongul Island, which is about 4 km

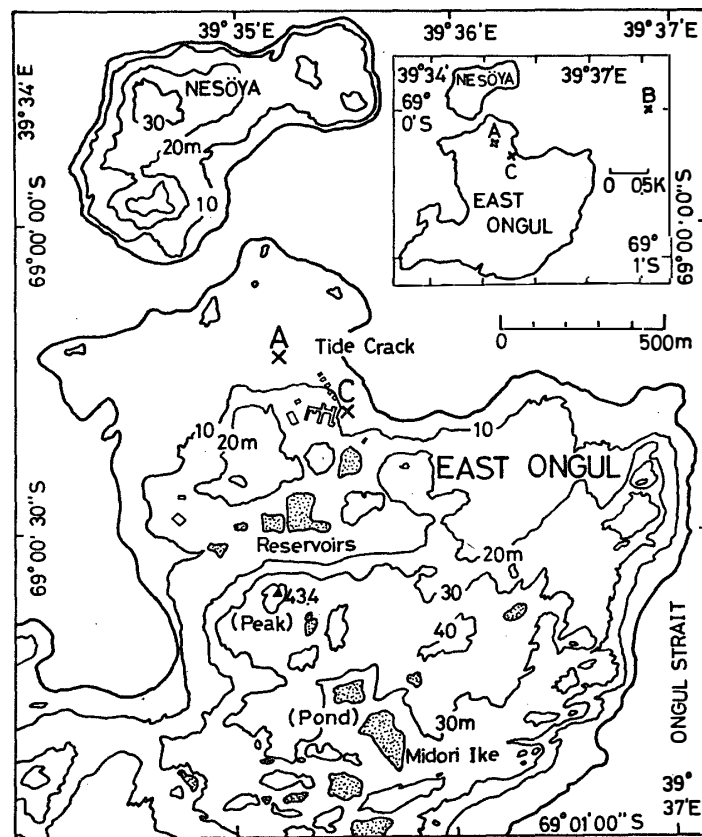


Fig. 1. Topography of the northeastern part of East Ongul Island and the location of the tower and the pole used in the micrometeorological observations.

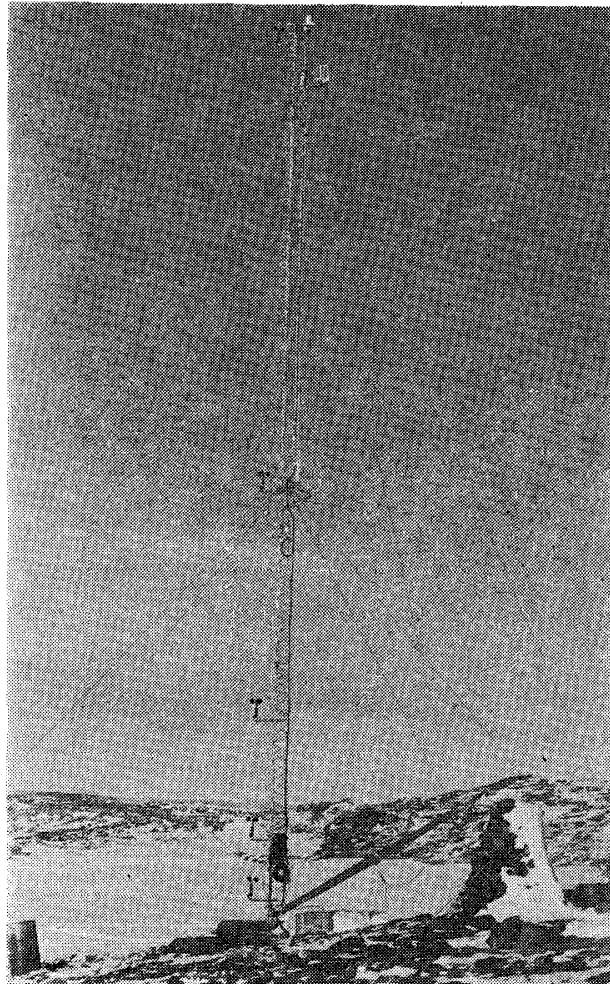


Fig. 2. Sonic anemometer-thermometers and the 21 m-high tower.

from the Antarctic Continent, has hills of 30 to 40 m high at about 300 m away from the observation site under the lee of the prevailing wind.

According to MURAKOSHI (1958), the prevailing wind direction at Syowa Station is northeast. The 21 m-high tower, made of iron pillars of an equilateral triangle shape with 30 cm span was decided upon for measuring the prevailing wind (Fig. 2).

A three-dimensional S.A.T. was set up on the tower at a height of 20 m. The sensor probe was attached to the beam so as to keep the probe 1 m away from a side of the tower to avoid its interference. The S.A.T. has probes with 20 cm span for the longitudinal, lateral and vertical wind speed components of the 120° crossing. The winds of N to E directions can be measured without any interference from the wakes of any transducers or supporting members (MITSUTA *et al.*, 1967; MITSUTA, 1971). The data of SSW, SE and ESE wind directions were included in this analysis, because a strong stable stratification was often found in these cases. The data of SW to WSW wind directions were excluded because of the interference effects. Underlines in Figs. 4

to 8, 11 and 13 indicate the data on winds blowing from the rear side of the S.A.T. The author sometimes checked the horizontal direction of the S.A.T. with a level, but it could not be always said that the horizontal direction is not changeable after a strong blizzard.

The S.A.T. used at Syowa Station was adjusted at -20°C as the standard point of the temperature correction in order to work under extremely low temperature conditions. The frequency response of the S.A.T. is 100 Hz. The electric signals from the S.A.T. were recorded on the four-channel rectigraph of 40 mm width (per channel) with 50 mm/s chart speed. The response time of the recorder is about 0.03 s. The sampling interval was 0.2 s for the wind speed fluctuation and the recording time for each run was 5 minutes.

Five sets of three-cup anemometer and of platinum resistance thermometer with shelter were installed on the tower respectively at the heights of 21, 10, 5, 2.5 and 1.25 m above the ground. The electric pulses due to the cup-rotation of the anemometers were counted by the magnetic digital counters and the electric output from the platinum resistance thermometers was recorded on an electric auto-balancing recorder. The data of 80 runs were obtained with the S.A.T. in this observation. And the data of 33 runs were analyzed in the present investigation. Table 1 summarizes the meteorological conditions at the time of observation. The wind speed observed by the S.A.T. is different from the wind speed observed by the three-cup anemometer at the height of 20 m for the longitudinal wind component, because the former is 5-minute mean and the latter is 10-minute mean or 20-minute mean.

In the present paper, the standard deviations (σ_U , σ_V and σ_W) of the longitudinal (U), lateral (V) and vertical (W) wind speed fluctuations were calculated from eq. (1), the Eulerian auto-correlation coefficients [$R_U(t)$, $R_V(t)$ and $R_W(t)$] of the three dimensional wind components from eq. (2) and the power spectral densities [$S_U(n)$, $S_V(n)$ and $S_W(n)$] of the three dimensional wind components from eq. (3).

The standard deviation, σ_U and the Eulerian auto-correlation coefficient, $R_U(t)$ of the longitudinal wind speed component are expressed respectively as follows:

$$\sigma_U = \left\{ \sum_{i=1}^N (\bar{u} - u_i)^2 / N \right\}^{1/2}, \dots\dots\dots (1)$$

and

$$R_U(t) = \sum_{i=1}^{N-p} (u'_i \cdot u'_{i+p}) / \sigma_U^2 (N-p), \dots\dots\dots (2)$$

where suffix i and p are integers 1, 2, 3 ... n ($n=300$ or 500), \bar{u} is the longitudinal mean wind speed (5 minutes), u the longitudinal wind speed, u' ($=\bar{u}-u_i$) the wind speed fluctuation, N the total number of data (1500), t ($=\Delta t p$) the time lag and Δt the sampling time interval (0.2 s).

The power spectral density, $S_U(n)$ of the longitudinal wind speed component is expressed as follows:

$$S_U(n_i) = \Delta t \sigma_U^2 \left\{ R_U(0) + 2 \sum_{i=1}^{M-1} R_U(t) \cos \frac{\pi p i}{M} + R_U(t) \cos \pi i \right\}, \dots\dots\dots (3)$$

Table 1. Summary of the associated meteorological conditions at Syowa Station in 1970.

Run	Date	Time	Wind velocity (m/s)						Air temperature (°C)			Weather, Amount of cloud		Wind direction
			U_{21}	U_{10}	U_5	$U_{2.5}$	$U_{1.25}$	S.A.T. U_{20}	T_{21}	T_{10}	$T_{1.25}$			
1	4 Apr.	1102-1112	6.67	5.67	5.25	4.92	4.50	6.55	- 6.8	- 7.0	- 7.2	☉	—	ENE
2	6 Apr.	0958-1010	4.80	4.00	3.43	3.15	2.93	6.93	- 8.3	- 8.3	- 8.7	☉	—	ENE
3	6 Apr.	2322-2334	6.39	5.25	4.86	4.42	4.03	6.56	-10.5	-10.7	-11.4	☉	—	E
4	13 Apr.	1659-1711	6.33	5.60	5.27	4.67	4.33	6.70	- 9.0	- 9.1	- 9.3	☉	—	NE
5	20 Apr.	0900-0912	5.08	4.00	3.42	2.83	2.33	5.49	-12.1	-12.6	-13.8	☉	—	NE
6	20 Apr.	2320-2342	7.78	6.11	5.56	4.78	4.55	8.75	-13.0	-13.4	-14.5	☉	—	ENE
7	6 May	1049-1103	8.33	7.67	7.00	6.83	6.50	8.41	- 5.0	- 5.2	- 5.4	☉	10	NE
8	8 May	1120-1133	5.95	5.32	5.00	4.68	4.44	6.07	- 8.4	- 8.6	- 8.7	☉	10	NE
9	9 May	1740-1752	1.0>	1.0>	1.0>	1.0>	1.0>	1.05	-22.0	-23.5	-26.2	☉	5	E
10	16 May	1105-1118	3.00	4.11	4.55	3.33	3.11	3.00	-16.8	-18.6	-20.5	☉	0	ESE
11	26 May	1610-1622	13.41	11.98	11.35	10.56	10.16	13.20	- 6.5	- 6.7	- 7.3	☉	10	NE
12	13 June	1047-1103	1.47	1.28	1.08	0.81	0.67	2.16	-33.3	-33.7	-34.2	☉	1	SSW
13	15 June	1600-1613	1.83	0.75	0.33	1.0>	1.0>	2.01	-20.1	-20.8	-21.5	☉	5	N
14	3 July	1134-1147	10.00	8.44	7.67	7.00	6.56	10.10	-11.0	-11.8	-12.9	☉	4	NE
15	10 July	1550-1605	14.47	12.80	12.13	11.27	10.73	14.42	-11.3	-11.9	-12.5	☉	2	ENE
16	10 July	1615-1625	13.78	12.22	11.44	10.67	10.00	15.00	-17.4	-18.2	-19.1	☉	2	ENE
17	3 Aug.	1024-1036	8.41	7.46	7.17	6.67	6.49	8.05	-18.4	-18.9	-19.1	☉	7	NNE
18	2 Sep.	1713-1727	2.33	2.00	1.85	1.67	1.67	3.78	-25.2	-25.8	-27.2	☉	4	SSW
19	5 Sep.	1050-1103	9.44	8.11	7.67	6.56	6.00	9.49	-17.8	-18.0	-18.2	☉	9	ENE
20	16 Sep.	1532-1544	2.83	2.28	1.94	1.75	1.61	4.72	-18.7	-19.3	-20.5	☉	0	E
21	25 Sep.	1540-1550	0.75	0.70	0.67	0.60	0.50	1.66	- 9.0	- 9.1	-10.5	☉	0	SE
22	29 Sep.	1505-1518	8.33	7.74	7.26	6.90	6.55	8.63	-14.8	-14.9	-15.0	☉	4	NNE
23	3 Oct.	1339-1352	23.56	21.56	20.67	18.89	18.00	24.11	- 3.5	- 3.9	- 4.4	☉	10	ENE
24	19 Oct.	1705-1718	14.04	12.72	12.11	11.40	10.88	17.06	- 7.7	- 7.8	- 8.2	☉	10	ENE
25	22 Oct.	2053-2103	1.94	1.67	1.53	1.94	1.81	2.41	-12.0	-12.2	-13.3	☉	0	E
26	29 Oct.	1118-1125	7.41	6.85	6.48	6.11	5.83	8.17	-11.5	-11.7	-12.0	☉	10	NNE
27	30 Oct.	1643-1656	17.29	15.52	14.85	13.65	13.12	19.49	- 8.1	- 8.3	- 8.7	☉	10	NE
28	10 Nov.	0953-1010	1.08	0.83	0.75	0.67	0.67	1.28	- 0.9	- 1.4	- 2.2	☉	0	NNE
29	11 Nov.	0010-0018	12.17	9.67	9.33	7.63	7.33	13.00	- 8.5	- 9.3	-10.2	☉	0	ENE
30	11 Nov.	1737-1745	4.27	4.06	3.65	3.44	2.50	3.50	- 3.6	- 3.7	- 4.1	☉	0	E
31	1 Dec.	1135-1148	16.98	15.10	13.90	12.92	12.29	19.62	+ 2.0	+ 1.7	+ 1.4	☉	10	NE
32	8 Dec.	2230-2243	7.73	6.67	5.71	5.00	4.76	4.29	- 1.6	- 2.0	- 2.4	☉	0	NE
33	9 Dec.	0826-0834	13.00	12.33	11.67	10.33	9.83	14.20	- 0.9	- 1.1	- 1.1	☉	0	E

Observations and Data Analyses

where i is integer $0, 1, 2 \dots n, n_i (= \pi i / M \Delta t)$ the frequency and M the maximum time lag.

Standard deviations σ_V and σ_W , Eulerian auto-correlation coefficients $R_V(t)$ and $R_W(t)$ and power spectral densities $S_V(n)$ and $S_W(n)$ of the lateral and vertical wind speed components are obtained with the same method.

In order to obtain the smooth distribution of the power spectral density, the averaging procedure which is known as Hamming Window (BLACKMAN and TUKEY, 1958) has been applied in this analysis. In the present paper, M and N for the longitudinal and lateral wind components are taken for 300 and 1500, and M and N for the vertical wind component are 500 and 1500, respectively.

The friction velocity (U_*) is calculated from

$$U_*^2 = - \sum_{i=1}^N (\bar{u} - u_i)(\bar{w} - w_i) / N, \dots\dots\dots (4)$$

where \bar{w} and w_i are the vertical mean wind speed and the vertical wind speed, respectively.

The Richardson number (Ri) is calculated from the vertical wind velocity gradient and the vertical air temperature gradient at the height of 20 m. Ri is defined by

$$Ri = \frac{g}{\theta} \frac{d\theta}{dZ} / \left(\frac{du}{dZ} \right)^2, \dots\dots\dots (5)$$

where g is the acceleration of gravity and θ the representative air temperature (absolute temperature) at the height of Z .

Observations show that for the small time lag, *i.e.*, $t < 3$ s the auto-correlation coefficient of the three dimensional wind components may be approximated by

$$R_j(t) = 1 - C_{kj} t^{m_j}, \dots\dots\dots (6)$$

where C_k and m are numerical constants and j is the longitudinal (U), lateral (V) and vertical (W) wind components. The value of m falls between 0.55 and 0.69 in the present paper. This formula yields the characteristic time scales of the three dimensional wind components,

$$T_j = (1/C_{kj})^{1/m_j}, \dots\dots\dots (7)$$

According to INOUE (1952) and INOUE *et al.* (1955), the scales of the "largest turbulon" of the longitudinal, lateral and vertical wind speeds (A_U, A_V and A_W) and of the "smallest turbulon" of the longitudinal wind speed (λ_U) may be expressed respectively as follows:

$$A_j = U_{20} T_j, \dots\dots\dots (8)$$

and

$$\lambda_U = (v^3/\varepsilon)^{1/4}, \dots\dots\dots (9)$$

where $v (= \mu/\rho)$ is the kinematic viscosity of the air, μ the molecular viscosity coefficient, ρ the air density and ε the energy dissipation rate of the turbulence.

Taking the similarity theory for the inertial subrange of turbulence or the range of intermediate turbulon, the following relation is given (INOUE *et al.*, 1955):

$$2\sigma_U^2\{1-R_U(t)\}=C_1\varepsilon^{2/3}(tU_{20})^{2/3}, \dots\dots\dots (10)$$

where C_1 is the numerical constant given experimentally to be 1.6. From eq. (10) the energy dissipation rate (ε) may be rewritten as follows:

$$\varepsilon=\left(\frac{2}{C_1}\right)^{3/2}\frac{\sigma_U^3\{1-R_U(t)\}^{3/2}}{tU_{20}}. \dots\dots\dots (11)$$

2.2. The meteorological data during the period from March 1970 to February 1971 are used in this analysis. Measurements of meteorological elements were carried out at the micrometeorological observation site.

The vertical profiles of wind velocity and air temperature were measured respectively with the five sets of three-cup anemometer and of platinum resistance thermometer at the same heights mentioned above. The wind data measured by an aerovane as the routine surface meteorological data are used in annual measurements of wind direction and wind velocity. The wind velocity and the wind direction by an aerovane at the height of 10 m are represented respectively the ten-minute mean and sixteen wind directions, *i.e.*, NNE is first and N is sixteenth with clockwise. The wind velocity is divided into some distribution classes, in which the wind velocity interval except for below 1 m/s is determined as 2 m/s. A dead calm indicates the wind velocity below 0.1 m/s and the mean values are the total mean. The air temperature in the routine surface observation (Japan Meteorological Agency, 1971) which was measured in the screen at the height of 1.5 m above the ground was used in the present analysis. Eight-run data obtained at the times of 3, 6, 9, 12, 15, 18, 21 and 24 o'clock were analyzed in the present paper.

The temperature gradient on the tower was obtained from the measurements at the heights of 10 m and 1.25 m. And the annual variations of the mean air temperatures at the heights of 20, 10 and 1 m (T_{20} , T_{10} and T_1), the annual variation of the tropospheric maximum air temperature (T_x), the altitude of ground inversion (H_x) (Japan Meteorological Agency, 1971), and the annual variations of T_x-T_1 , $T_{20}-T_1$ and $T_{10}-T_1$ were analyzed. The mean air temperature under the condition of ground inversion was used in the present analysis. The tropospheric maximum air temperature was obtained from the values of the aerological observations at 0300 o'clock (local time) at Syowa Station.

Considering the characteristics of the climate at Syowa Station, four seasons were defined as follows; the spring period is October and November, the summer period December, January and February, the autumn period March and April and the winter period May, June, July, August and September.

2.3. Vertical profiles of wind velocity, air temperature and snow temperature were observed on the smooth terrain of the sea ice about 2 km east of Syowa Station (Fig. 1) during the period from August 20th to September 19th, 1970. The 6 m-high pole (Fig. 3) for measuring the wind velocity was set up at point B. The terrain is the middle part of the Ongul Strait and has no obstacles within about 1 km from the

observation place. Five sets of three-cup anemometer (electro magnetic anemometer) were installed at the heights of 6, 3, 1.5, 0.8 and 0.4 m. As no source of A.C. electric power could be obtained, measurements of air temperature and snow temperature were carried out with stem thermometers and L tube thermometers every hour, referring to the air temperature profile and the snow temperature profile. Air temperatures were measured at the heights of 4, 2, 1, 0.5 and 0 m, and snow temperatures at the depths of 5, 10, 20, 30 and 50 cm. Table 2 shows some of the profiles.

LILJEQUIST (1957) presented an equation of the wind velocity profile which is applicable to various stratifications ranging from slightly stable to super-stable. The equation is as follows:

$$U_6 = U_A + U_L, \dots\dots\dots (12)$$

where U_6 is the mean wind velocity at the height of 6 m as the reference wind velocity, U_A the adiabatic component of wind velocity corresponding to the logarithmic law of the wind velocity profile for neutral stability in eq. (13), and U_L the linear component of wind velocity proportional to the height above the snow surface. The typical profile of wind velocity in strong stable stratification is shown in Fig. 33.

When the stratification is nearly neutral and the wind is blowing stationarily, the

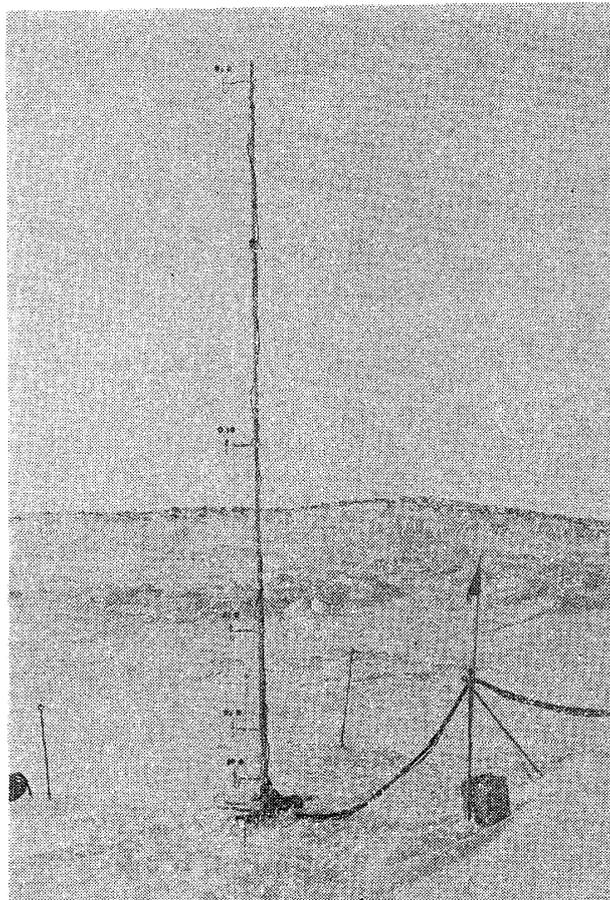


Fig. 3. Small three-cup anemometers and the 6 m-high pole.

Table 2. Summary of the associated meteorological conditions at point B above the sea ice in 1970.

Date	Time	Wind velocity (m/s)					Air temperature (°C)				Weather, Amount of cloud	
		U_6	U_3	$U_{1.5}$	$U_{0.8}$	$U_{0.4}$	T_4	T_2	T_1	T_0		
23 Aug.	2158-2209	3.89	2.77	2.08	1.76	1.39	-31.3	-32.5	-33.5	-35.6	○	0
23 Aug.	2226-2243	4.19	3.45	2.74	2.31	1.91	-31.4	-32.0	-32.3	-34.8	○	0
24 Aug.	0000-0010	1.07	0.80	0.59	0.46	0.38	-32.5	-33.1	-33.6	-35.2	○	0
27 Aug.	2328-2341	1.39	1.11	0.87	0.75	0.63	-31.7	-32.4	-33.3	-34.2	○	0
28 Aug.	2159-2210	1.77	0.82	0.41	0.29	0.24	-31.0	-32.0	-32.5	-34.0	○	0
28 Aug.	2250-2314	1.29	0.85	0.74	0.65	0.50	-27.4	-29.2	-30.5	-34.4	○	0
29 Aug.	0008-0027	1.21	0.87	0.69	0.57	0.39	-31.9	-32.4	-33.1	-34.7	○	0
29 Aug.	1323-1335	1.36	1.04	0.79	0.59	0.45	-28.9	-28.8	-29.5	-31.2	○	5
31 Aug.	1213-1223	1.65	1.18	0.93	0.80	0.67	-30.2	-31.0	-31.8	-33.4	○	1
31 Aug.	1741-1802	2.21	2.00	1.76	1.10	0.89	-34.0	-35.0	-36.4	-39.2	○	0
31 Aug.	2144-2200	2.51	2.33	2.01	1.57	1.20	-31.5	-33.8	-37.2	-40.1	○	0
1 Sep.	0000-0010	1.66	1.38	1.12	0.79	0.46	-32.3	-32.8	-33.8	-40.4	○	0
1 Sep.	0647-0700	0.96	0.61	0.46	0.40	0.38	-32.8	-33.0	-33.5	-40.2	○	0
1 Sep.	1151-1207	1.62	1.44	1.17	0.90	0.64	-29.2	-30.1	-30.7	-34.5	○	1
1 Sep.	1258-1313	1.23	0.93	0.75	0.59	0.43	-24.5	-25.9	-27.7	-34.1	○	0
3 Sep.	1547-1607	5.35	4.89	4.34	3.89	3.48	-19.3	-19.8	-20.8	-25.1	⊕	0
4 Sep.	0512-0518	5.85	5.05	4.55	4.11	3.70	-12.7	-12.8	-13.2	-14.6	⊕	0
7 Sep.	1653-1711	1.64	1.15	0.71	0.43	0.35	-30.6	-31.4	-32.3	-35.4	○	0
7 Sep.	1754-1802	2.19	1.53	0.88	0.60	0.39	-31.7	-33.6	-34.3	-36.5	○	1
7 Sep.	2059-2111	3.05	2.12	1.70	1.44	1.11	-34.9	-35.5	-35.8	-37.4	○	1
8 Sep.	0001-0011	1.00	0.63	0.31	0.21	0.20	-33.2	-34.0	-35.1	-38.0	○	1
8 Sep.	0345-0355	2.33	1.70	1.30	0.83	0.66	-29.5	-30.2	-30.9	-36.0	○	6
8 Sep.	0356-0409	4.21	3.45	2.93	2.54	2.13	-27.7	-29.3	-30.1	-33.4	○	7
10 Sep.	0007-0022	3.68	2.97	2.69	2.43	2.12	-23.8	-23.8	-24.1	-25.5	⊙	10
13 Sep.	1738-1802	1.45	1.15	0.87	0.70	0.49	-31.0	-32.0	-32.7	-36.0	○	0
13 Sep.	2030-2058	1.85	0.99	0.62	0.52	0.30	-31.7	-33.8	-35.4	-38.9	○	0
14 Sep.	0110-0130	2.72	2.02	1.54	1.27	1.04	-33.4	-33.7	-34.5	-39.0	○	1
14 Sep.	0158-0206	1.98	1.45	1.21	1.09	0.92	-33.1	-33.8	-34.8	-38.1	○	1
17 Sep.	1351-1405	3.85	3.36	2.95	2.66	2.36	-20.5	-19.0	-20.6	-22.0	○	0
18 Sep.	2004-2023	3.67	2.72	2.18	1.83	1.52	-24.0	-24.5	-25.5	-29.5	○	1

Observations and Data Analyses

wind velocity is represented by the logarithmic law equation, *i.e.*,

$$u = \frac{U_*}{\kappa} \ln \frac{Z}{Z_0}, \quad \dots \dots \dots (13)$$

where κ is the Kármán constant.

Neglecting the molecular transfer of momentum (*cf.*, SUTTON, 1953), the friction drag (τ) is expressed as follows:

$$\tau = \rho l^2 \frac{du}{dZ} \bigg| \frac{du}{dZ} \bigg| = \rho K_M \frac{\partial u}{\partial Z}, \quad \dots \dots \dots (14)$$

where ρ is the air density, l the mixing length and K_M the momentum diffusion coefficient. The friction velocity (U_*) is obtained from τ and the logarithmic law.

Now, k is assumed as follows:

$$k = U_L / U_6 \quad \dots \dots \dots (15)$$

According to eqs. (12), (14) and (15), the momentum diffusion coefficient in stable stratification is represented by the following equation:

$$K_M = \frac{U_*^2}{\frac{\partial u}{\partial Z}} = \frac{(1-k)Z_6 U_6^2}{\left(\ln \frac{Z_6}{Z_0}\right) \left(\frac{Z_6}{Z+Z_0} + \frac{k}{1-k} \ln \frac{Z_6}{Z_0}\right)}, \quad \dots \dots \dots (16)$$

where Z_6 is the reference height of 6 m. Then, the mixing length in stable stratification (l_s) is expressed as follows:

$$l_s = \frac{k(Z+Z_0)}{1 + \frac{k}{1-k} \frac{Z_6}{Z_0} \ln \frac{Z_6}{Z_0}} \quad \dots \dots \dots (17)$$

Furthermore, the Richardson number in eq. (5) in stable stratification (Ri_s) is rewritten as follows:

$$Ri_s = \frac{S \left(\frac{Z_6}{U_6} \ln \frac{Z_6}{Z_0}\right)^2}{(1-k)^2 \left(\frac{Z_6}{Z+Z_0} + \frac{k}{1-k} \ln \frac{Z_6}{Z_0}\right)^2} \quad \dots \dots \dots (18)$$

The stability ratio (S) is represented as follows:

$$S = \frac{g}{\theta} \frac{\partial \theta}{\partial Z} \quad \dots \dots \dots (19)$$

The observation of visibility was carried out during the period from March to August, 1970. Air temperatures during the observation with the drifting snow were between -5°C and -20°C .

In order to observe the visibility for a short distance, two groups of flags were used. One was a row of flags set at intervals of 25 m in distance from 25 m to 150 m in the open space of the heliport. The other was the flags previously set at the points of 13, 21 and 40 m. The visibility for a long distance was obtained from the distances of several objects such as the Transmitter Hut (about 400 m), Miharashi Iwa (about 1 km), the ice cliff on the east coast of the Ongul Strait (about 4 km) and so on.

The wind velocity measurement was made on the smooth snow surface at point A in Fig. 1. The aerodynamic roughness length (Z_0) obtained from the vertical wind velocity profiles was used in computations of friction drag (τ) and friction velocity (U_*) for $-0.01 < Ri < 0.05$, *i.e.*, nearly neutral stratification. The wind velocity data in March and April were used for the analysis of the wind velocity profile under nearly neutral conditions. The wind velocity was counted by the magnetic digital recorder in the Glaciology Laboratory.

Now, the author explains the turbulent heat transfer on the sea ice. One of the observations was carried out during the period from July 14th to 18th and the other from August 20th to September 19th, 1970. The observation when the sun did not rise, was carried out at point A about 150 m north of the Air-Traffic Control Hut. On the other hand, the observation during which the sun rose the horizon for about 8 to 12 hours a day was carried out on the sea ice at point B. The observations of wind velocity, air temperature and snow temperature have been already mentioned above.

At the height of 1.5 m the minimum air temperature was -42.2°C in the former period of observations and -41.0°C in the latter period.

3. Observation Results

3.1. Characteristics of atmospheric turbulence in stable stratification at Syowa Station

3.1.1. Wind above the sloping terrain and standard deviation of wind speed fluctuation

Fig. 4 (A) shows the relation between W_{20}/U_{20} and Ri in eq. (5). According to this figure, the ratio of W_{20}/U_{20} is independent of Ri . The relation between U_{20} and W_{20} is expressed by

$$W_{20}=0.330U_{20}.$$

The physical meaning of this relation is not very clear. It must be noted that the observation site has the inclination of about 10 degrees. The comparatively large coefficient of this relation seems to be due to the drifting snow and the property of the geographical slope, because the measured wind on this tower becomes the updraft wind which blows toward East Ongul Island from a smooth sea ice or a spill-over wind in reverse.

When the wind, especially the prevailing wind, blows from the east direction over the smooth sea ice surface, the measurements of wind velocity influence the updraft effect. As the iron tower is grounded at the height of 8 m above the sea level and East Ongul Island has hills of 30 to 40 m height, it seems that the wind velocity of the lower atmospheric surface layer on wind velocity profiles is strong as compared with the upper layer, especially in the case of the prevailing wind.

The relation between U_{20} and Ri is shown in Fig. 4 (B). This relation is expressed as follows:

$$U_{20}=3.10Ri^{-0.56}.$$

Fig. 5 (A) shows the relations between σ_j ($j=U, V, W$) and Ri and Fig. 5 (B) the relations between σ_j/U_{20} ($j=U, V, W$) and Ri . The empirical formulae may be expressed as follows:

$$\sigma_U=0.45Ri^{-0.35}, \sigma_V=0.37Ri^{-0.35} \text{ and } \sigma_W=0.60Ri^{-0.48},$$

and

$$\sigma_U/U_{20}=0.16Ri^{0.22}, \sigma_V/U_{20}=0.13Ri^{0.22} \text{ and } \sigma_W/U_{20}=0.23Ri^{0.15}.$$

The relations between σ_U and Ri and between σ_V and Ri have the same gradient. Standard deviations of the longitudinal, lateral and vertical wind speed fluctuations

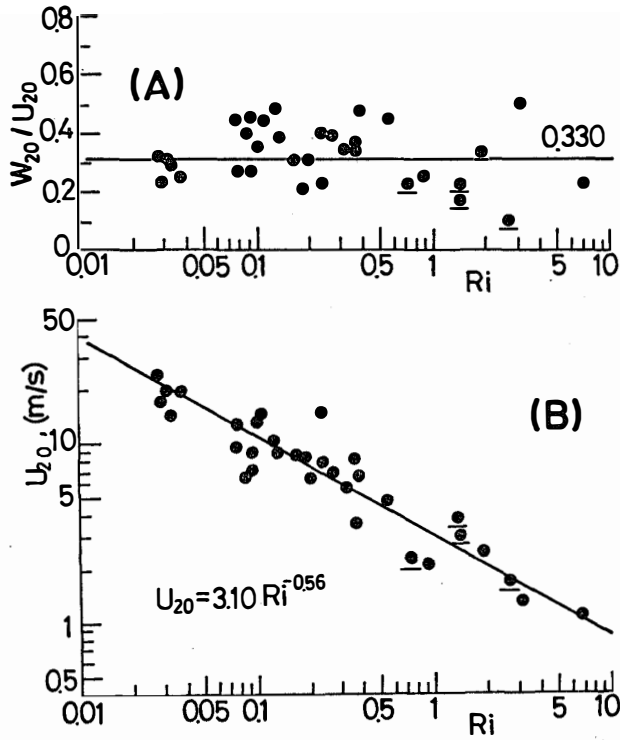


Fig. 4. (A) Relation between the Richardson number (Ri) and the ratio of the vertical mean wind speed (W_{20}) to the longitudinal mean wind speed (U_{20}) at the height of 20 m. (B) Relation between Ri and U_{20} . Points with underline indicate the data of winds blowing from the rear side of the S.A.T. (Figs. 4 to 8, 11 and 13).

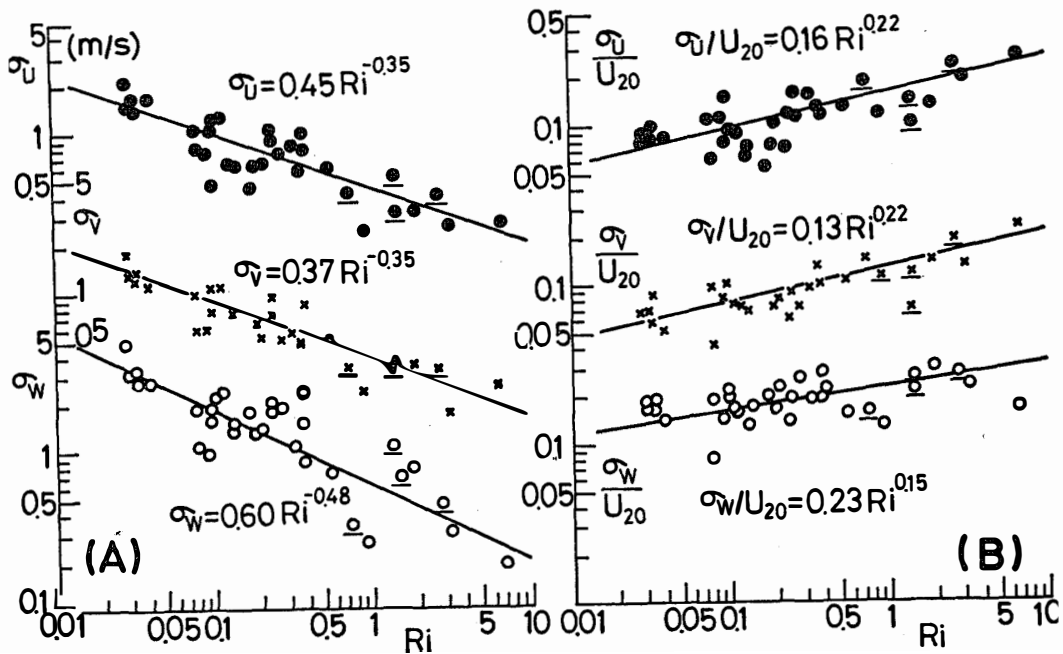


Fig. 5. (A) Variations of standard deviations of the longitudinal, lateral and vertical wind speed fluctuations (σ_U , σ_V and σ_W) against Ri . (B) Variations of ratios of σ_U , σ_V and σ_W to U_{20} (σ_U/U_{20} , σ_V/U_{20} and σ_W/U_{20}) against Ri .

decrease exponentially with the increase of Ri . It seems to be due to the reason mentioned above that the value of σ_w is rather large.

3.1.2. Gustiness and gust factor against U_{20}

The gustiness is defined as σ_U/U_{20} and the gust factor U_m/U_{20} , where U_m is the maximum instantaneous wind speed for five minutes. The relation between σ_U/U_{20} and U_{20} is rewritten from the relation σ_U and U_{20} . And the relation between the gustiness and U_{20} shown in Fig. 6 (A) is expressed as follows:

$$\sigma_U/U_{20} = 0.240U_{20}^{-0.48}, \text{ for } 0 < U_{20} \leq 8.5 \text{ m/s}$$

and

$$\sigma_U/U_{20} = 0.086, \text{ for } U_{20} \geq 8.5 \text{ m/s.}$$

The transition wind speed in this figure may be estimated at about 8.5 m/s at the height of 20 m, which is equivalent to about 8.0 m/s at the height of 10 m. It was reported by LILJEQUIST (1957) and MAKI (1971) that the drifting snow begins to start at about 8.0 m/s at the height of 10 m. This value seems to correspond to the wind speed at which snow particles begin to drift.

The relation between the gust factor and U_{20} is shown in Fig. 6 (B) and expressed as follows:

$$U_m/U_{20} = -0.30 \log U_{20} + 1.60, \text{ for } 0.5 < U_{20} < 50 \text{ m/s.}$$

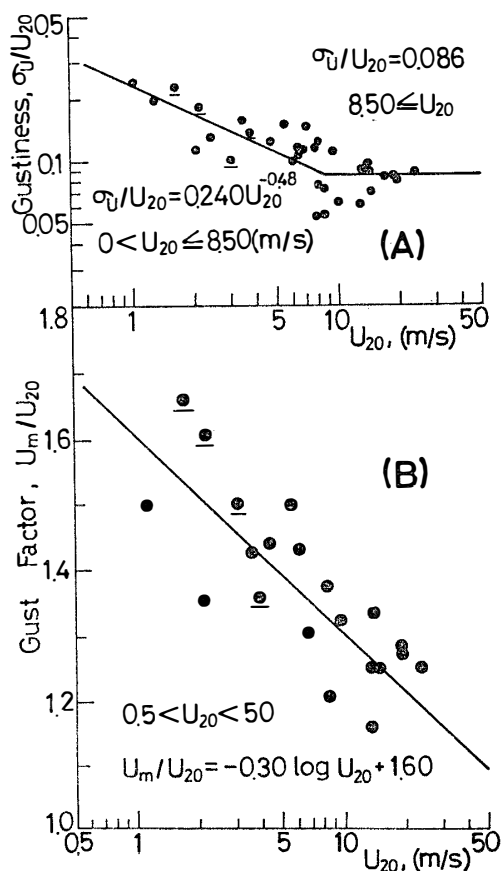


Fig. 6. (A) Variation of the ratio of σ_U to U_{20} (σ_U/U_{20} , gustiness) against U_{20} . (B) Variation of the ratio of maximum instantaneous wind speed for 5 minutes to U_{20} (U_m/U_{20} , gust factor) against U_{20} .

The gust factor decreases with the increase of U_{20} . In the present paper the sampling time is five minutes, and the value of gust factor increases with the increase of the sampling time.

3.1.3. Relations between Ri and ratios of standard deviations to friction velocity

The ratios of σ_U/U_* , σ_V/U_* and σ_W/U_* as a function of Ri are shown in Fig. 7. U_* is obtained from eq. (4). There are no obvious dependencies of σ_U/U_* , σ_V/U_* and σ_W/U_* on the stability (Ri) in stable stratification, i.e.,

$$\sigma_U/U_* = 1.80, \sigma_V/U_* = 1.55 \text{ and } \sigma_W/U_* = 3.00.$$

Comparing the present results obtained above the sloping terrain with other results above the flat surface, the values of σ_U/U_* and σ_V/U_* are somewhat smaller than the values 1.9–2.8 hitherto obtained by MONIN (1962). On the other hand, the present

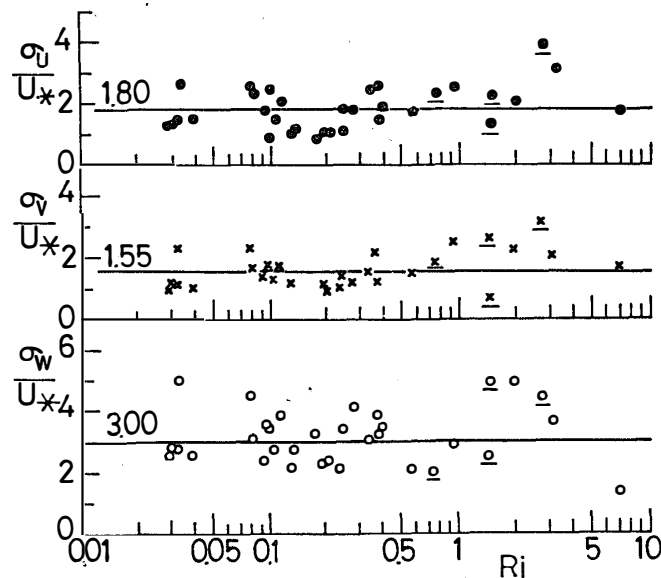


Fig. 7. Ratios of standard deviations of the longitudinal, lateral and vertical wind speed fluctuations to the friction velocity (σ_U/U_* , σ_V/U_* and σ_W/U_*) against Ri .

ratio of σ_W/U_* is somewhat larger than the values 0.5–1.2 obtained by MONIN (1962), 1.1 by SHIOTANI (1963), 1.7 by BUSCH and PANOFSKY (1968) and 0.2–3.0 by YOKOYAMA (1971). Furthermore, BUSINGER *et al.* (1969) reported the relation that σ_W/U_* increases with the decrease of Ri in unstable stratification.

The fairly small values of σ_U/U_* and σ_V/U_* and the fairly large value of σ_W/U_* in the present paper might be attributed to the updraft and spill-over effects depending on the topography of the Syowa Station area.

3.1.4. Energy dissipation rate

It is known theoretically that the energy dissipation rate (ϵ) in neutral stratifica-

tion is proportional to the third power of the wind velocity.

In the present paper, the relation between ε/U_{20}^3 and Ri is shown in Fig. 8, where ε is obtained from eq. (11).

The relation is expressed by the following equation:

$$\varepsilon/U_{20}^3 = 4.2 \times 10^{-5} Ri^{0.53}.$$

According to this equation, ε is proportional to the third power of U_{20} and to about the 0.5 power of Ri in stable stratification.

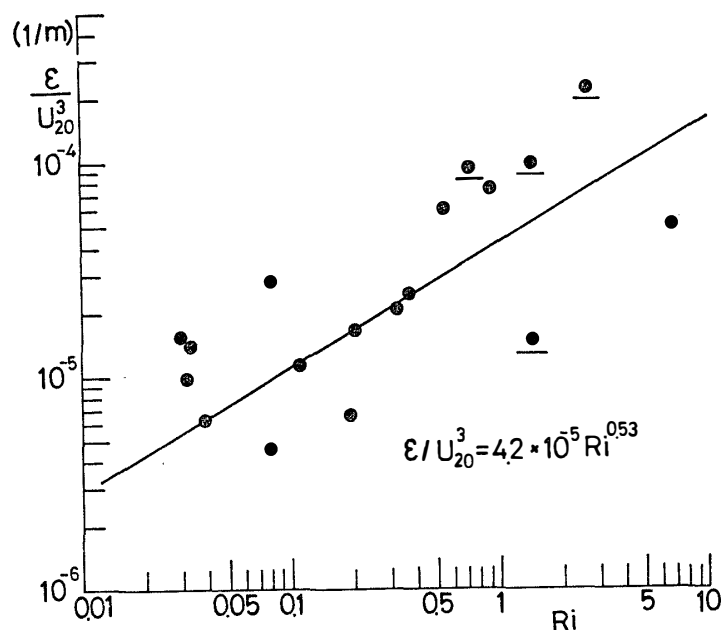


Fig. 8. Ratio of energy dissipation rate to the third power of the longitudinal mean wind speed at the height of 20 m (ε/U_{20}^3) against Ri .

3.1.5. Frequency distribution of wind speed

The following three groups of typical meteorological data are distinguishable by the weather conditions, such as the presence or absence of drifting snow and the strength of wind velocity, namely by the degree of stability. The groups are as follows:

Group S (super-stable winds); runs 9, 10, 18, 21, 25 and 28.

Group K (katabatic winds); runs 14, 15, 16, 26, 29 and 33.

Group B (blizzard winds); runs 11, 23, 24, 27 and 31.

Group S, e.g., run 9 ($Ri=6.82$) is characterized by super-stable stability with gentle wind and non-drifting snow, group K, e.g., run 29 ($Ri=0.080$) by moderate stable stability with fairly strong wind and low drifting snow, and group B, e.g., run 23 ($Ri=0.029$) by slightly stable stability with strong wind and high drifting snow.

Fig. 9 shows the frequency distributions of the longitudinal, lateral and vertical

wind speeds. In this figure, the scale intervals of wind speeds are different from each other, *i.e.*, 0.2 m/s for super-stable winds, 0.5 m/s for katabatic winds and 1.0 m/s for blizzard winds.

The value of the peak in the frequency distribution of the lateral wind speed is the highest of the three and the distribution range is not wide, so to speak, "a thin pattern"; on the other hand, that of the vertical wind speed is the lowest of the three and the distribution range is wide, so to speak, "a thick pattern" except May 9th. This frequency distribution is similar to Gaussian error curve, but the peak of the distribution has a tendency to shift toward the regions of high wind speed in this figure. It is

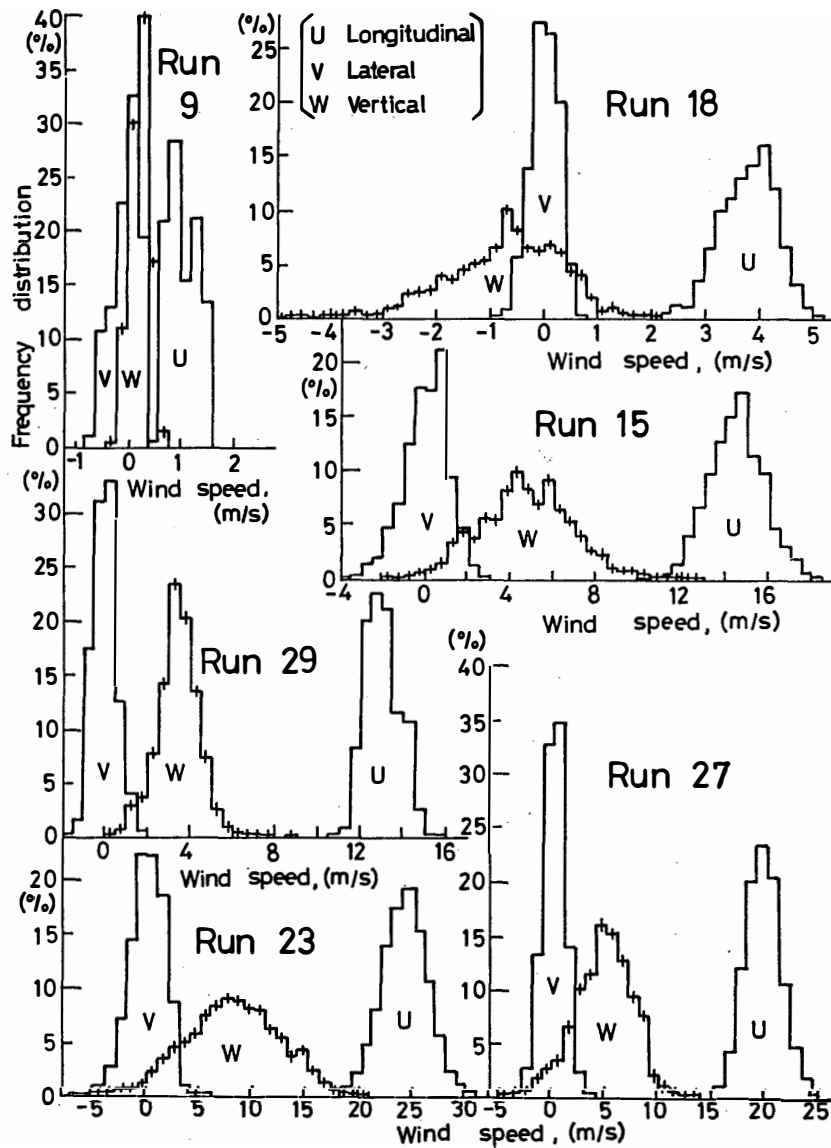


Fig. 9. Frequency distributions of the longitudinal, lateral and vertical wind components in super-stable winds, katabatic winds and blizzard winds.

interesting that the gradient of reduction on the right side of the peak is steeper than that on the left side, though the reason is not clarified as yet.

As the updraft wind direction has a positive sign on the vertical wind speed, the peak of the vertical wind speed in run 18 is represented as a negative wind speed, *i.e.*, the SSW wind blows down from an upper part in East Ongul Island.

3.1.6. Eulerian auto-correlation coefficient

As examples of Eulerian auto-correlation coefficients, $R_U(t)$, $R_V(t)$ and $R_W(t)$ are shown in Fig. 10. Characteristic times of the longitudinal, lateral and vertical wind speeds (T_U , T_V and T_W) are obtained by the extrapolation method using the tendency in the range from 0.2 s to about 3.0 s according to the relation between t and $1-R_j(t)$ ($j=U, V, W$). By the use of eqs. (6) and (7) for a small time lag of $0.2 < t < 3.0$ s, we can obtain the characteristic times (T_U , T_V and T_W) as shown in Table 3.

Table 3. Characteristic times of the longitudinal, lateral and vertical wind components, T_j ($j=U, V, W$) obtained from eqs. (6) and (7).

T_j and ratio Run	T_U (s)	T_U/T_W	T_V (s)	T_V/T_W	T_W (s)
8	13.2	5.28	3.60	1.44	2.50
9	500.	6.94	123.	1.71	72.0
10	65.0	6.50	24.0	2.40	10.0
15	4.70	5.00	1.80	1.91	0.94
17	11.0	5.79	3.00	1.58	1.90
18	26.0	5.65	7.40	1.61	4.60
19	7.60	5.24	3.20	2.21	1.45
21	100.	10.87	32.0	3.48	9.20
23	2.55	3.40	1.10	1.47	0.75
26	14.5	7.63	4.80	2.53	1.90
27	8.50	8.10	1.95	1.86	1.05
29	7.10	5.46	2.70	2.08	1.30
31	5.80	5.27	1.65	1.50	1.10
33	7.50	6.52	1.60	1.39	1.15
Mean		6.26		1.94	

From the table, the ratio of $T_U : T_V : T_W$ is represented as (3.4–10.9) : (1.4–3.4) : 1 and the mean ratio is 6.3 : 1.9 : 1. The ratio $T_U/T_W=6.3$ is smaller than $T_U/T_W=10$ reported by INOUE *et al.* (1955). Characteristic times (T_U , T_V and T_W) for group S are larger than those for group K or group B. According to these results, the mean scale of the “largest turbulon” represents a solid body like a long and narrow cubic vortex having the dimensions of length : breadth : height=6.3 : 1.9 : 1.

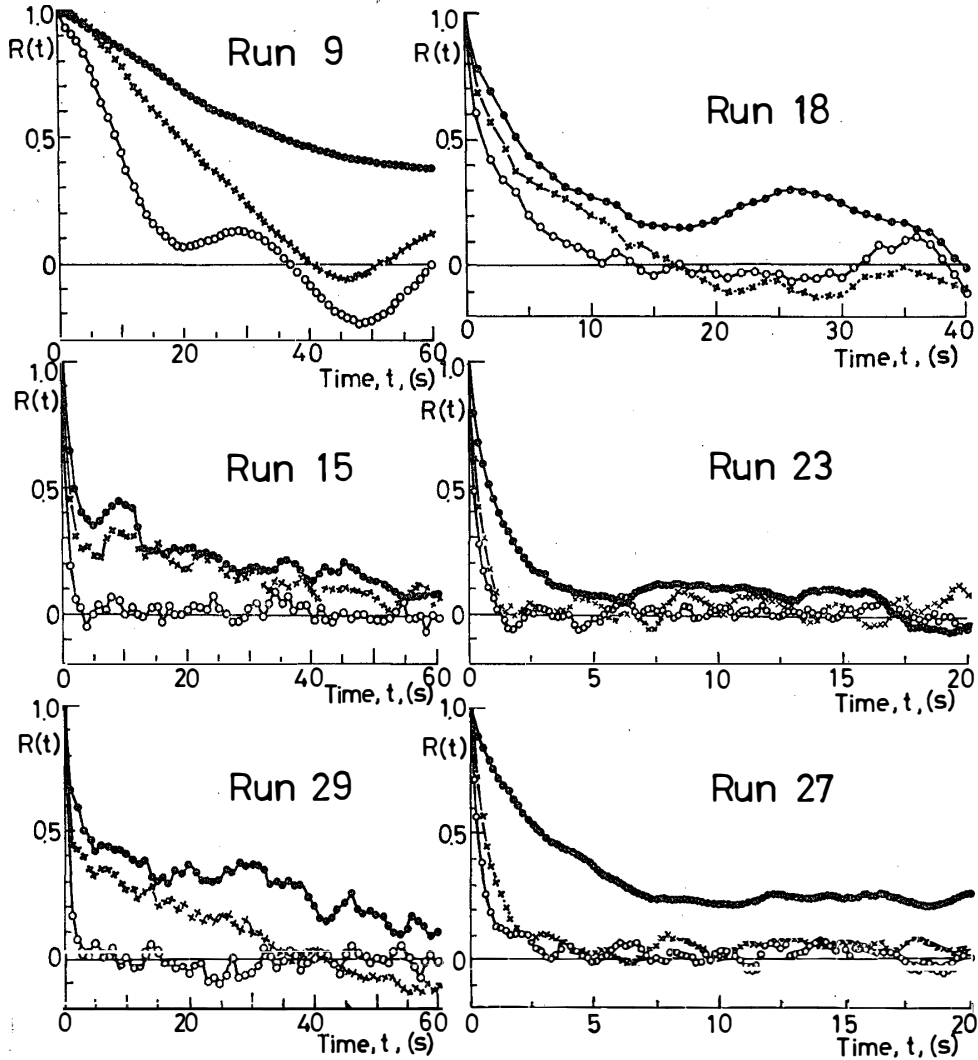


Fig. 10. Eulerian auto-correlation coefficients of the longitudinal, lateral and vertical wind speeds [$R_U(t)$, $R_V(t)$ and $R_W(t)$] against the time lag (t) in super-stable winds, katabatic winds and blizzard winds.

3.1.7. Scale of turbulence

The scales of the "largest turbulon" of the longitudinal, lateral and vertical wind speeds (A_U , A_V and A_W) are obtained from eq. (8). Fig. 11 (A) shows the values of A_U , A_V and A_W as a function of Ri . These results are not much indicative because the data of different wind directions were included. The empirical formulae except for the data in super-stable stratification in run 9 seem to be as follows:

$$A_U=107, A_V=33.0 \text{ and } A_W=17.0.$$

In this figure the value of A_U may be seen to increase slightly with the increase

of Ri , but in consideration of the trends of Λ_V and Λ_W , the scales of Λ_U , Λ_V and Λ_W seem to be independent of the stability for $Ri < 3.0$. These constant values show the ratio $107:33.0:17.0 \doteq 6.3:1.9:1$, which represents a cubic vortex with length : breadth : height = $6.3:1.9:1$. The present value of Λ_U is almost coincident with the results by WEBB (1955) and BATCHELOR (1956). According to INOUE *et al.* (1955), the scale of the

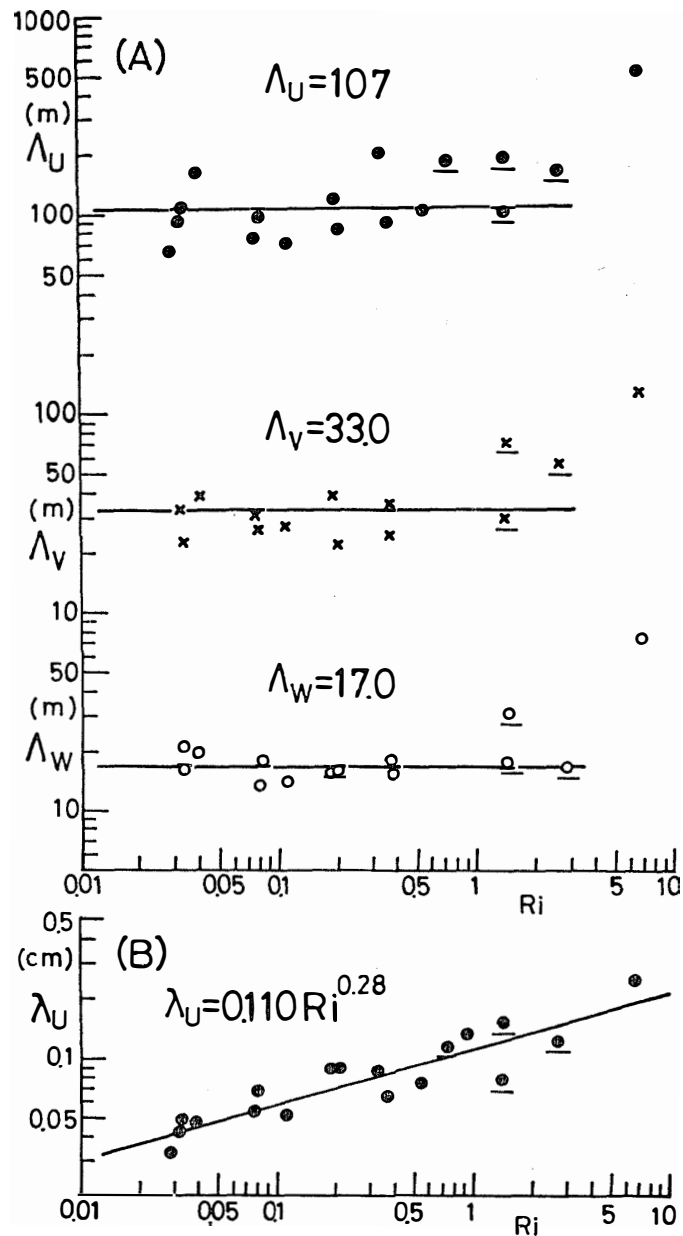


Fig. 11. (A) Scales of the largest turbulon of the longitudinal, lateral and vertical wind speeds (Λ_U , Λ_V and Λ_W) against Ri .
(B) Scale of the smallest turbulon of the longitudinal wind speed (λ_U) against Ri .

largest turbulon of the longitudinal wind speed is about ten times as large as the observation height, whereas in the present observation, the scale is about three to ten times as large. The scale of turbulence, especially for horizontal wind speed, varies with the sampling time.

The scale of the "smallest turbulon" of the longitudinal wind speed (λ_U) is obtained from eq. (9). λ_U is theoretically equal to the scales of the "smallest turbulon" of the lateral and vertical wind speeds (λ_V and λ_W). The value of λ_U in terms of Ri is represented in Fig. 11 (B). The empirical formula is as follows:

$$\lambda_U = 0.110 Ri^{0.28}.$$

The value of λ_U increases exponentially with the increase of Ri . The coefficient of this equation is about 10^{-5} times as large as the value of A_U .

According to the value of exponent in eq. (6), KOLMOGOROFF obtained $2/3$ with the similarity theory as the value of m . INOUE *et al.* (1955) reported that the value $2/3$ was observed with the small-scale Robinson cup-anemometer, while $1/3$ was obtained in a good many cases. SHIOTANI (1953) obtained $2/3$ empirically with the hot-wire anemometers. KOBAYASHI and ISHIDA (1970) reported that the value of m falls between $1/3$ and $2/3$, and the values of $2/3$ are not many. In the present paper, the value of m falls between 0.55 and 0.69 except for the data of winds blowing from the rear side of the S.A.T.

3.1.8. Power spectral density and maximum spectral density

Fig. 12 shows some examples of power spectral densities of wind speed fluctuations. A $-5/3$ power law is seen at the nondimensional frequency of $nZ/U_{20} > 1.0$.

In run 9 ($Ri=6.82$), the power spectral densities of the longitudinal, lateral and vertical wind speeds decrease sharply in the frequency range between 0.2 and 0.5 c/s. The stronger the wind velocity, the higher becomes the frequency to which the $-5/3$ power law is applicable.

Now, the peaks of power spectral densities (${}_U n_p$, ${}_V n_p$ and ${}_W n_p$) denote the frequencies, at which the power spectral densities of the longitudinal, lateral and vertical wind speeds [$nS_U(n)$, $nS_V(n)$ and $nS_W(n)$] have their respective maximum. The present result is coincident with LUMLEY and PANOFKY's (1964) result showing that the values of ${}_U n_p$, ${}_V n_p$ and ${}_W n_p$ decrease with the increase of stability.

It was shown by BUSCH *et al.* (1968) that the value becomes smaller in the order of $nS_U(n)$, $nS_V(n)$ and $nS_W(n)$ in the range of $nZ/U_{92} < 0.2$ (U_{92} is the wind velocity at the height of 92 m).

BUSINGER *et al.* (1969) obtained several results on normalized vertical spectra under neutral and slightly stable conditions. These results are not coincident with the tendencies of vertical spectra in katabatic or blizzard winds, but almost with the tendencies of vertical spectra under super-stable conditions. Furthermore, SOMA (1964) reported that in strong winds (typhoon) the value of ${}_U n_p$ is small, being about 0.02 or 0.1 c/s at the height of 26 m.

The dependencies of nondimensional frequencies of the longitudinal, lateral and vertical wind speeds (${}_U n_p Z/U_{20}$, ${}_V n_p Z/U_{20}$ and ${}_W n_p Z/U_{20}$) on the stability of Ri are

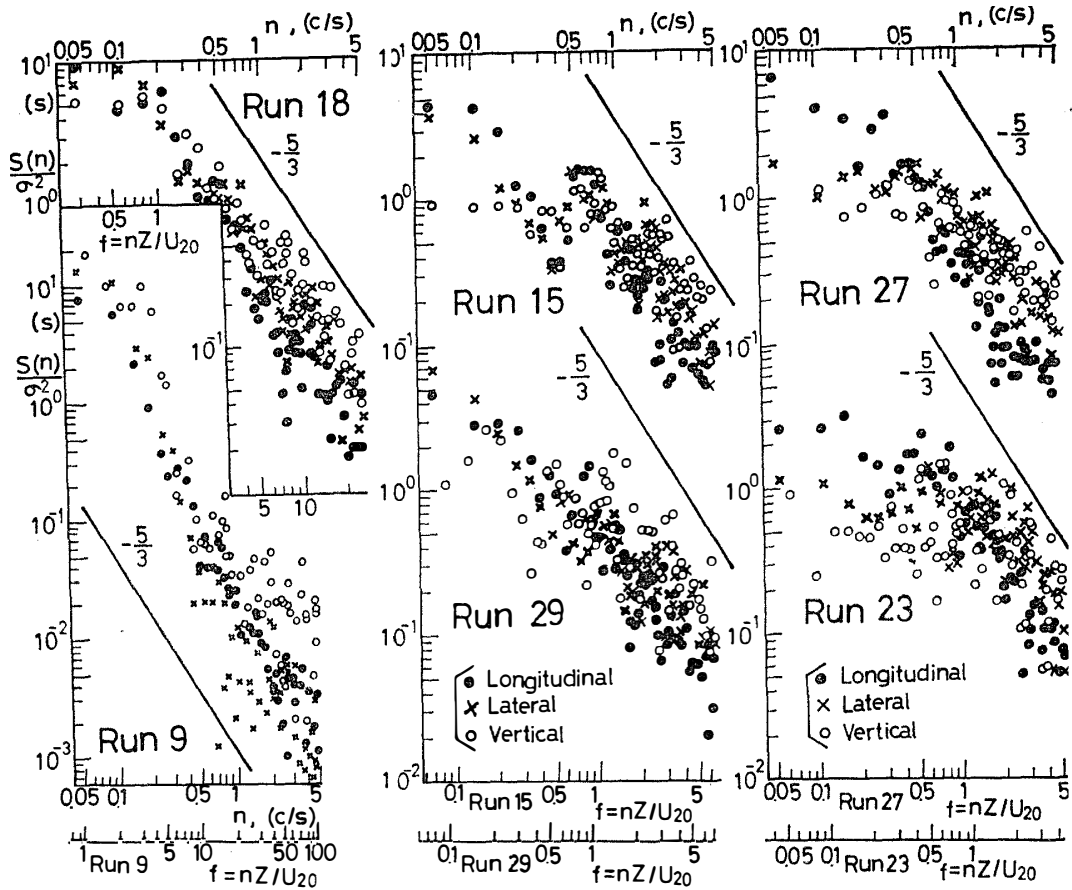


Fig. 12. Power spectral densities $[S_U(n), S_V(n)$ and $S_W(n)]$ against the frequency (n) and the nondimensional frequency (nZ/U_{20}) in super-stable winds, katabatic winds and blizzard winds.

obtained as follows:

$$u n_p Z/U_{20} = 1.05 Ri^{0.21}, \quad v n_p Z/U_{20} = 1.80 \quad \text{and} \quad w n_p Z/U_{20} = 2.80 Ri^{-0.32}.$$

The results are shown in Fig. 13. With the increase of Ri , the value of $u n_p Z/U_{20}$ for the longitudinal wind speed increases exponentially and the value of $w n_p Z/U_{20}$ for the vertical wind speed decreases exponentially. For the lateral wind speed, however, the value of $v n_p Z/U_{20}$ is independent of stability in strong stable stratification for $0.02 < Ri < 7.0$. On the other hand, KAIMAL *et al.* (1972) reported that nondimensional frequencies of the longitudinal, lateral and vertical wind speeds at the maximum spectral densities increase with the increase of Z/L [L is the MONIN-OBUKHOV (1954) length] in slightly stable stratification for $Z/L < 1.7$ ($Ri \approx 0.2$) at the heights of 5.66, 11.3 and 22.6 m. BUSINGER *et al.* (1969) reported that $w n_p Z/U_4$ (U_4 is the wind speed at the height of 4 m) increases with the increase of Ri in unstable stratification.

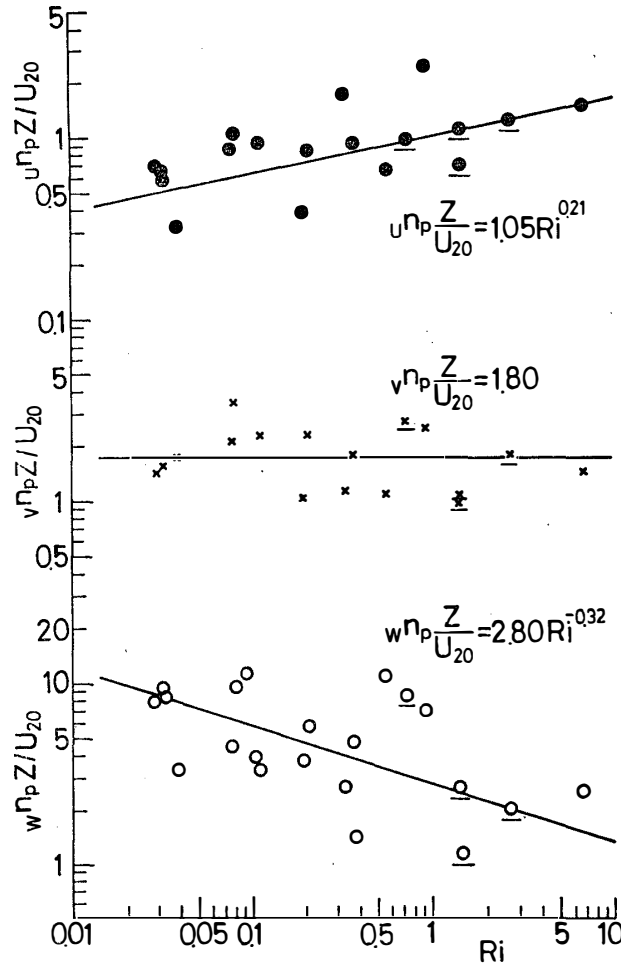


Fig. 13. Nondimensional frequencies, at which the power spectral densities of the longitudinal, lateral and vertical wind speeds have their respective maximum values ($U_p^n Z / U_{20}$, $v_p^n Z / U_{20}$ and $w_p^n Z / U_{20}$) against Ri.

3.2. Statistical analyses of general meteorological elements at Syowa Station

3.2.1. Frequency distribution of 16 wind directions (Fig. 14)

The frequency distribution of 16 wind directions by season shown that the prevailing wind directions of NNE, NE, ENE and E take up about 50 to about 70 percent (%), of which NE occupies 19–29% which is a maximum in every season.

In winter, the frequency of prevailing wind directions is not very large, whereas that of southern wind directions is larger than in other seasons, namely, SSE amounts to about 10%. As a matter of fact, the frequency of southern wind directions (S and SSE) is larger and the wind velocity is stronger than in other seasons. This is attributable to an outbreak from the antarctic anticyclone which accelerates the lowering of

air temperature in winter. The frequencies of southern wind directions in spring and autumn fall in an intermediate region between the summer-value and the winter-value, and the frequencies of prevailing wind directions are almost the same in spring, summer and autumn.

The frequency of the dead calm (below 0.1 m/s) is 12–13% in winter, about 5% in spring, about 8% in autumn and below 1% in summer. In other words, the dead calm and the stable stratification are found more often in winter than in other seasons. In summer, the dead calm is not often but the breeze (above 0.1 m/s and below 3.0 m/s) is more often than in other seasons, and the mean wind velocity becomes smaller.

3.2.2. Frequency distribution of mean wind velocity for 16 wind directions (Fig. 15)

The mean wind velocity in summer is generally smaller than in other seasons, but the prevailing wind directions are NE, ENE and E, similar to those in other seasons. The total mean wind velocity in summer is slightly below 5 m/s, smaller than that in other seasons which is about 6.5 m/s. In winter, on the other hand, the total mean wind velocity is similar to that in spring and autumn. Nevertheless, the wind velocities of NE and ENE directions in the prevailing winds in winter are above

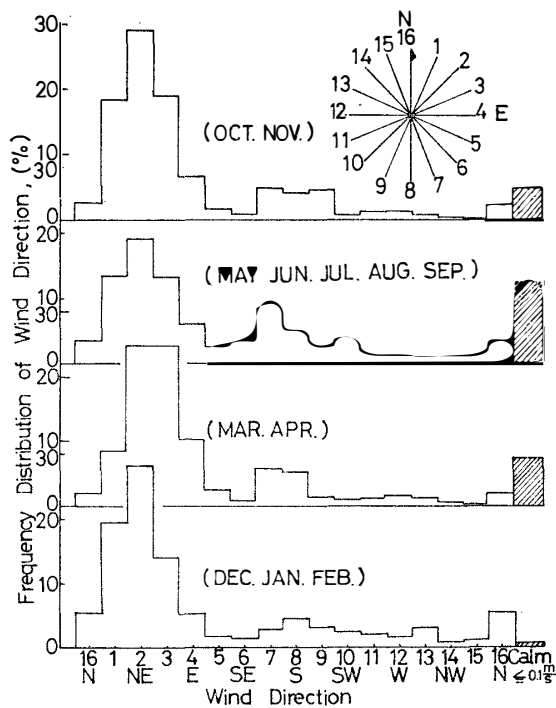


Fig. 14. Frequency distribution and the seasonal variation of 16 wind directions.

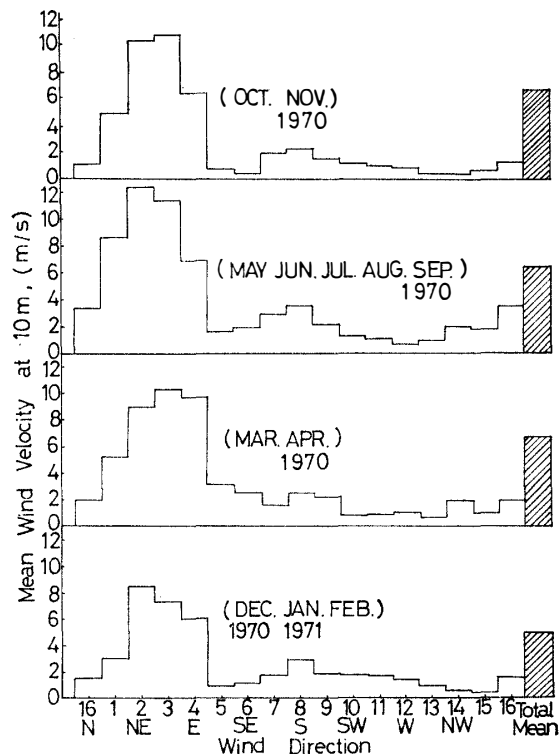


Fig. 15. Frequency distribution and the seasonal variation of mean wind velocity for 16 wind directions.

11 m/s, larger than in other seasons. The prevailing wind directions in spring and autumn are NNE to E, the wind velocities of ESE to N directions are generally low and those of southern wind directions are slightly high.

The wind velocity of prevailing winds is relatively lower in March, September, December, January and February. Particularly, the mean wind velocity is low in January although 45.0 m/s was recorded as the instantaneous wind velocity. The highest mean wind velocity of NE and ENE directions in the prevailing winds is about 14 m/s recorded in May and June. The mean wind velocity of S direction is higher in May (about 5 m/s) and in August (about 4 m/s). The seasonal mean wind velocity of southern directions influenced by values in May and August is larger than that in other seasons.

The monthly mean wind velocity is higher in April, May and October, and lower in September, December and January. According to YAMAZAKI *et al.* (1969), the monthly mean wind velocity is higher in March, April and November and lower in September, December, January and February. In some cases, the higher value of the monthly mean wind velocity appears one month earlier than the record of YAMAZAKI *et al.* (1969), but in most cases the results are nearly identical.

3.2.3. Frequency distribution of air temperature for 16 wind directions (Fig. 16)

In summer, the discrepancy of air temperature by the wind direction is generally insignificant, but in winter, the air temperatures of NNE to E wind directions are high, particularly high for the NE wind direction as it rises over -13°C . This high temperature is the reason that an atmospheric disturbance increases and the degree of ground inversion decreases with the increase of wind velocity. On the other hand, the low air temperatures of SSW and SW wind directions are due to an outbreak from the antarctic anticyclone and even the mean air temperature is -25°C . This is probably because the wind velocities of SSW and SW are not stronger than those of S and SSE and the air mass is cooled down with the nocturnal radiation while the wind blows above Ongul Island.

According to SEINO and SUZUKI (1964), the surface air layer and the tropospheric lower layer are controlled by the cold anticyclone accompanied by the ground inversion in winter when the atmospheric circulation of SE wind is somewhat active. However, when the cyclone disturbance appears at Syowa Station, the wind direction changes to NE and the air temperature increases rapidly.

The temperature variations in spring and autumn show a mixed pattern of summer-type and winter-type. The air temperature deviation by the wind direction is not significant except for the lower temperatures of SW and WSW in spring. In autumn, the air temperatures of NE, ENE and E are higher than the total mean air temperature and are similar to the winter's variation pattern. In spring and autumn, the air temperature of WNW is extremely high, apparently influenced by the direct solar radiation.

The air temperature of the dead calm (below 0.1 m/s) is lower on the whole, and the temperature gradient is larger than the total mean temperature gradient except

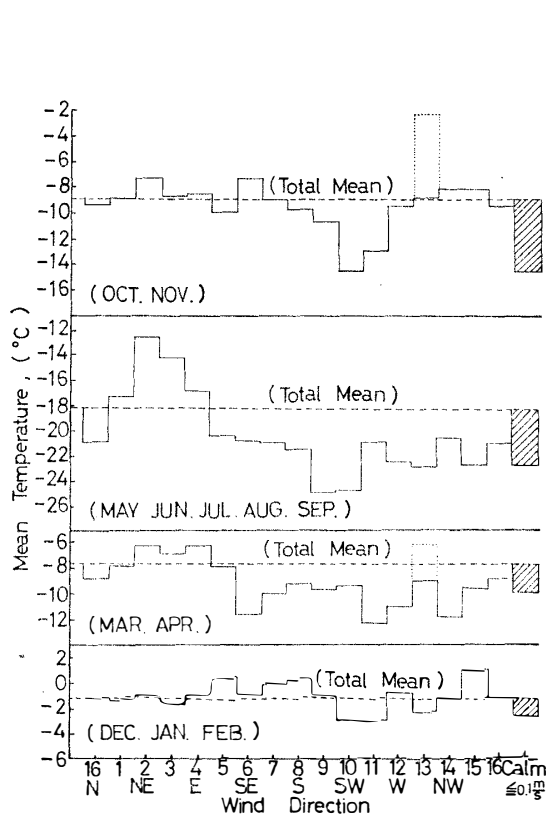


Fig. 16. Frequency distribution and the seasonal variation of air temperature for 16 wind directions.

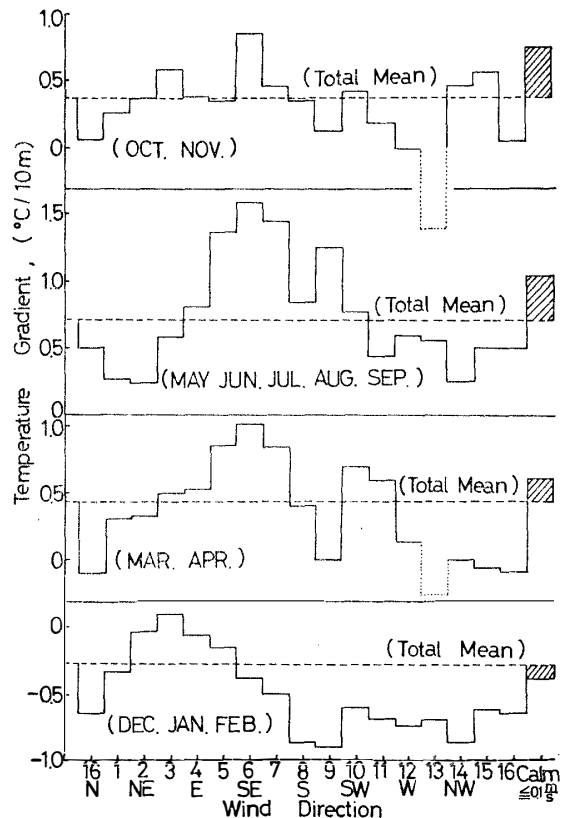


Fig. 17. Frequency distribution and the seasonal variation of vertical air temperature gradient for 16 wind directions.

in summer. The monthly air temperature distribution for the wind direction in July is not much different from the seasonal tendency, however, the air temperatures of SSW and SW are extremely low. The mean minimum air temperatures are -33°C by SSW and -31°C by SW. In summer, the monthly mean air temperatures of ESE, SE, SSE, S, NE and NNW are higher than 0°C , probably because of the rise of air temperature where the ground is not covered with snow or ice on Ongul Island.

3.2.4. Frequency distribution of vertical air temperature gradient for 16 wind directions (Fig. 17)

In winter, the vertical air temperature gradient (temperature gradient) for 16 wind directions is positive and shows stable stability. Particularly, the temperature gradients in the cases of ESE to SSW wind directions represent the super-stable stability, as the maximum mean gradient in winter is 1.5°C per 10 m and the temperature gradient in the case of S wind direction in July is 2.8°C per 10 m. However, the temperature gradients in the cases of NNE, NE and NW are rather small, and those in the cases of

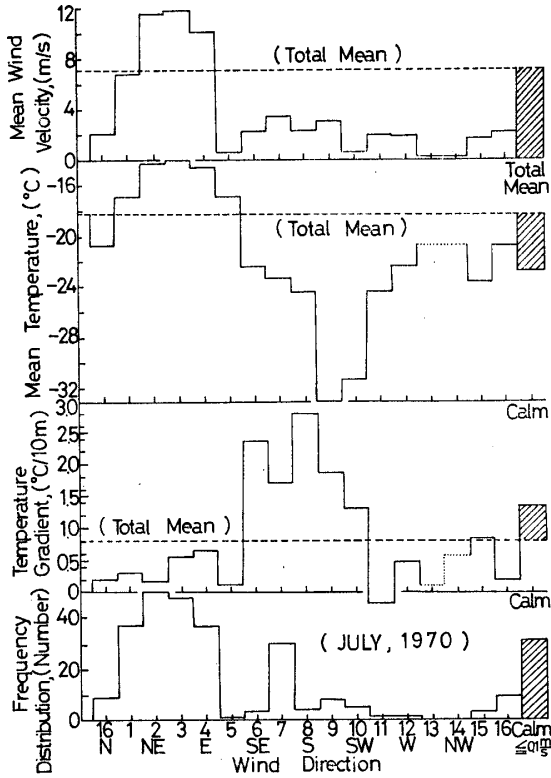


Fig. 18. Variations of wind velocity, air temperature, vertical air temperature gradient and the frequency distribution for 16 wind directions in July 1970.

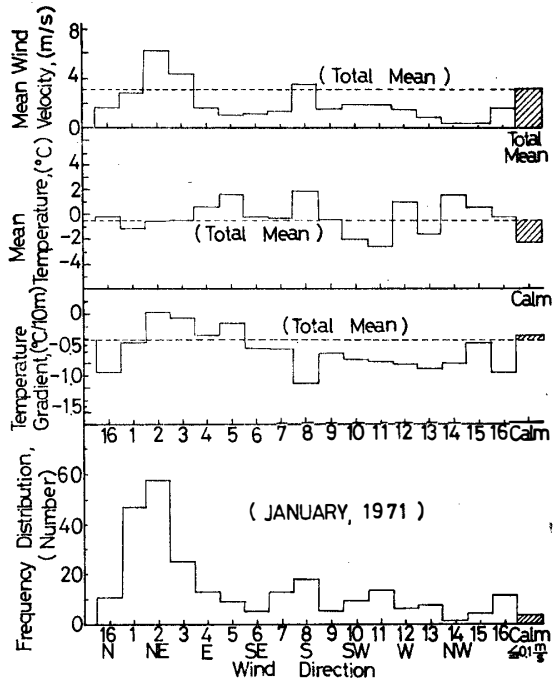


Fig. 19. Variations of wind velocity, air temperature, vertical air temperature gradient and the frequency distribution for 16 wind directions in January 1971.

SSE, S, SSW and SW are larger, but the air temperatures in the cases of SE, SSE and S are not very low.

In summer, the temperature gradients in the cases of NE to ESE wind directions are smaller and those of other wind directions have negative (unstable) sign as a whole except that the temperature gradient in the case of ENE has positive (stable) sign. This situation is just reverse to that of winter. It is understood that the snow and ice surfaces on Ongul Island become narrower in summer and the temperatures of the rock surface and sand soil surface rise to 20–30°C on a calm and clear day (MATSUDA, 1964) due to the direct solar radiation.

Furthermore, on a calm and clear day in summer the unstable stratification increases with the decrease of wind velocity. On the other hand, when the wind blows above the sea ice, the stable stratification can be maintained even in summer. The patterns in spring and autumn have a mixed characteristic of summer-type and winter-type. The temperature gradients in the cases of WNW to N show unstable stratification. In such a case as that mentioned in the section 3.2.3, only the temperature gradient in the case of WNW has negative sign. This fact is interesting but its cause is not

clear.

Now, the frequency distributions against 16 wind directions in July 1970 and January 1971 are shown in Figs. 18 and 19 as the typical monthly relations in Figs. 14, 15, 16 and 17.

3.2.5. Frequency distribution of wind velocity (Fig. 20)

On the whole, the frequency of the wind velocity below 3.0 m/s is very high. Especially in summer it reaches the maximum 55.5% and in autumn the minimum 41.4%. The frequency of the wind velocity below 1 m/s has its maximum of 33.7% in winter, and minimum of 24.4% in autumn. In other words, the frequency on a calm and clear day in winter is rather high. The frequency of stronger winds with the wind velocity 5.1–15.0 m/s is rather high in autumn. The frequencies of wind velocities 3.1–30.0 m/s gently decrease from 10% to 0% and the decrease pattern is not so different with other seasons.

The frequency distributions of wind velocities in July 1970 and January 1971 are shown in Fig. 24(A). In July, the frequencies of wind velocities 1.1–13.0 m/s and 15.1–27.0 m/s have respectively about 9% and about 1.5% for each interval. In January, the frequencies of 0–1.0 m/s and 1.1–3.0 m/s are 35% and 33% respectively. The

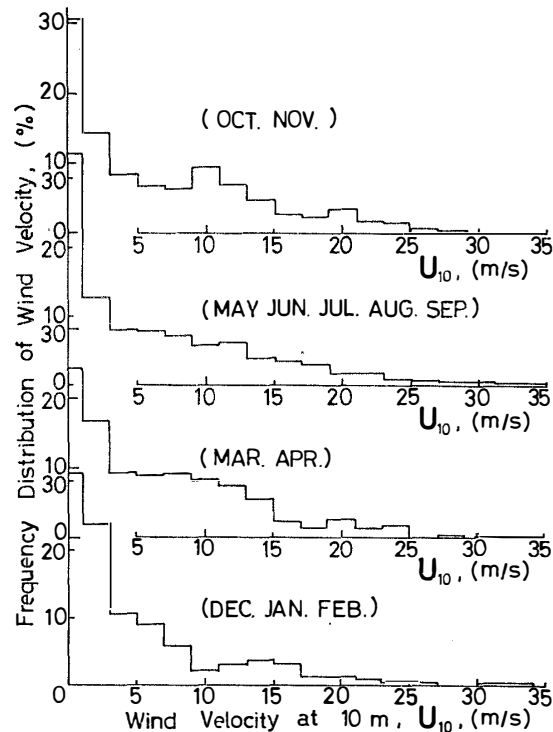


Fig. 20. Frequency distribution and the seasonal variation of wind velocity.

frequency of 1.1–3.0 m/s in January appears to be much higher than that in other months, which suggests that the probability of a calm and clear day is large.

3.2.6. Relation between U_{10} and mean air temperature and annual variation of warming ratio (Fig. 21)

The relation between U_{10} and the mean air temperature is shown in Fig. 21. It is very interesting that the mean air temperature increases with the increase of wind velocity at the height of 10 m (U_{10}). The warming ratio which is defined as the ratio of the increase of air temperature to the increase of wind velocity shows a significant annual variation. The warming ratio is 2.9°C per 10 m/s in spring, 1.3°C in summer, 3.0°C in autumn and 5.0°C in winter. The relations by four seasons are given as follows:

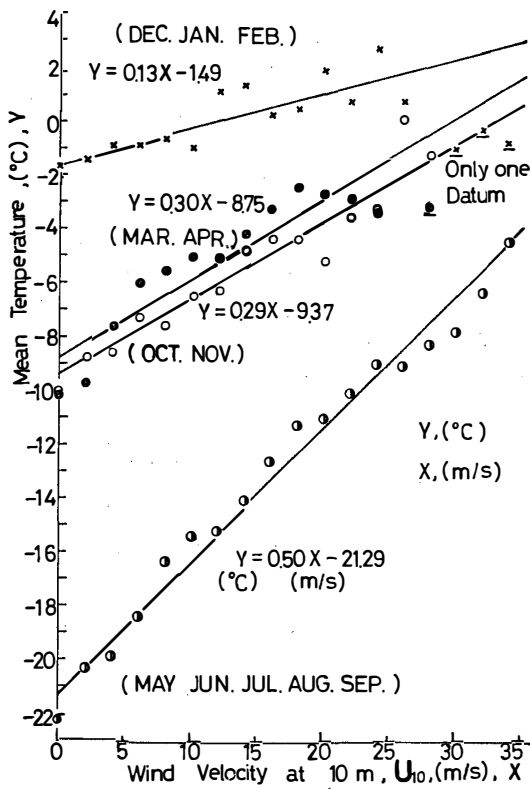


Fig. 21. Relation between the wind velocity at the height of 10 m (U_{10}) and the mean air temperature and its seasonal variation. Each point with underlines indicates the data having the single value respectively.

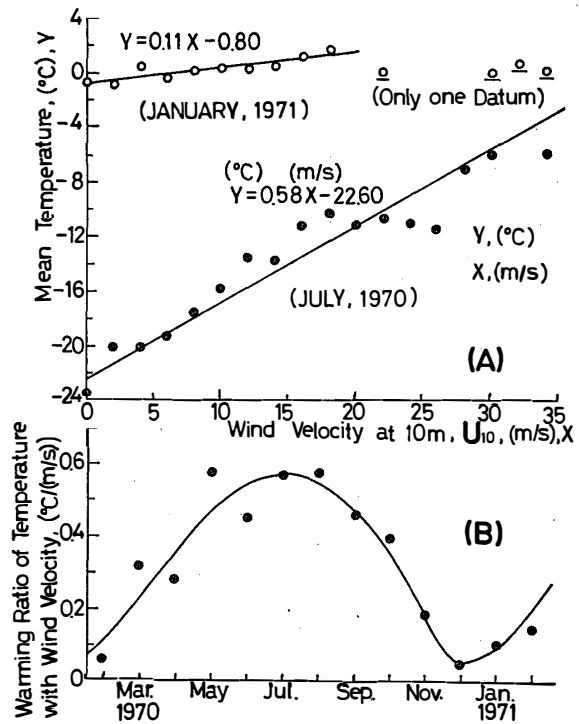


Fig. 22. (A) Relations between the wind velocity at the height of 10 m (U_{10}) and the mean air temperature in July 1970 and January 1971. (B) Relation between U_{10} and the mean air temperature and the annual variation of the warming ratio.

Spring; $Y=0.29X-9.37$,

summer; $Y=0.13X-1.49$,

autumn; $Y=0.30X-8.75$,

and

winter; $Y=0.50X-21.29$,

where Y is the air temperature ($^{\circ}\text{C}$) and X the wind velocity (m/s).

In summer, each class of the frequency distribution of the wind velocity over 30 m/s has only one datum. These data are due to the same phenomenon shown in the next section and are excluded from the present analysis as abnormal numerals.

The relations in July 1970 and January 1971 are expressed in Fig. 22 (A). The relations are represented as follows:

July 1970; $Y=0.57X-22.60$,

and

January 1971; $Y=0.11X-0.80$,

where Y is the air temperature ($^{\circ}\text{C}$) and X the wind velocity (m/s).

The annual variation of the warming ratio in Fig. 22 (B) shows a pattern reverse to that of mean air temperature. The maximum value of the warming ratio is 5.8°C per 10 m/s, about 10 times as large as the minimum value of 0.5°C per 10 m/s in Fig. 22 (B). It is clear that the air temperature increases with the increase of wind velocity. This is probably because the atmospheric disturbance and the advection current of heat appear with the increase of wind velocity and the degree of ground inversion decreases relatively.

3.2.7. Relation between U_{10} and vertical air temperature gradient (Fig. 23)

In winter, the vertical air temperature gradient decreases rapidly with the increase of wind velocity up to 10 m/s at U_{10} , and decreases gently above 10 m/s, and at 28 m/s it changes from stable to unstable *i.e.* nearly neutral stability. In summer, the variation pattern is almost reverse to the winter's pattern, and the temperature gradient increases with the increase of wind velocity below 8 m/s, and at 8 m/s it changes from unstable to stable, and settles at slightly stable stability.

It is considered that the decrease of unstable stability against the increase of wind velocity is due to the increase of air temperature of the atmospheric surface layer, as the ground surface is warmed by the direct solar radiation. On the other hand, when the cold wind influenced by the temperature of the sea ice blows toward the observation site, the unstable stability changes to nearly neutral stability.

The variation tendency of the relation between the temperature gradient and the wind velocity in nearly neutral stratification is explained as follows; when the wind velocity is low, there is sufficient time for air mass on Ongul Island to be warmed up, but if the wind velocity is over 8 m/s at U_{10} , cold air mass is directly observed at the observation site.

With the wind velocities over 30 m/s in summer in Fig. 23 and over 20 m/s in Fig. 24 (B), the values of temperature gradients observed on January 13th, 1971, were much larger than the other values. The instantaneous wind velocity observed on that

day was 45.0 m/s. This is ascribed to the day's unusual weather condition when the blizzard carried snow or ice particles from the sea ice surface, and the transported particles directly hit the platinum resistance thermometers. The stability apparently increases with the lowering air temperature of the lower atmospheric surface layer, becoming nearly 0°C. Judging from that the observation data under unusual weather conditions have the single value respectively, these data are excluded from the present analysis as abnormal numerals.

In spring, the temperature gradient has an almost constant value of 0.4°C per 10 m with the wind velocity below about 10 m/s, and decreases gently with the wind velocity over 10 m/s. In autumn, on the other hand, the temperature gradient decreases with the wind velocity of about 3 to about 10 m/s and the value becomes constant, about 0.3°C per 10 m, with the wind velocity over 10 m/s.

The variation patterns in July and January, shown in Fig. 24(B), are similar to those in summer and winter. Furthermore, it is interesting that the transition points of temperature gradients are found in the region of the wind velocity of 8 to 10 m/s

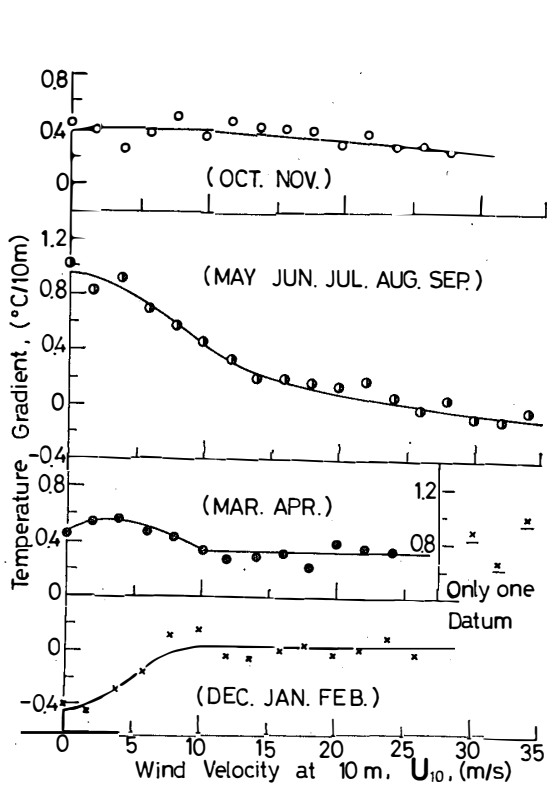


Fig. 23. Relation between the wind velocity at the height of 10 m (U_{10}) and the vertical air temperature gradient and its seasonal variation.

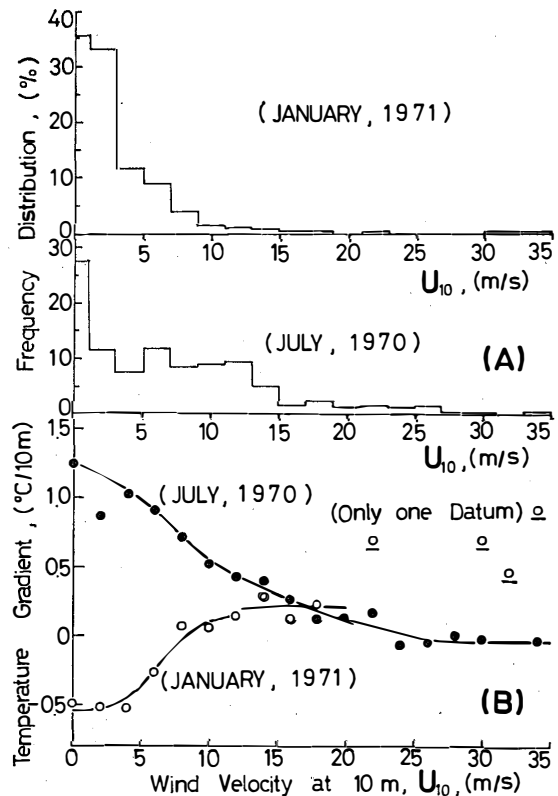


Fig. 24. (A) Frequency distributions of wind velocities in July 1970 and January 1971. (B) Relations between the wind velocity and the vertical air temperature gradient in July 1970 and January 1971.

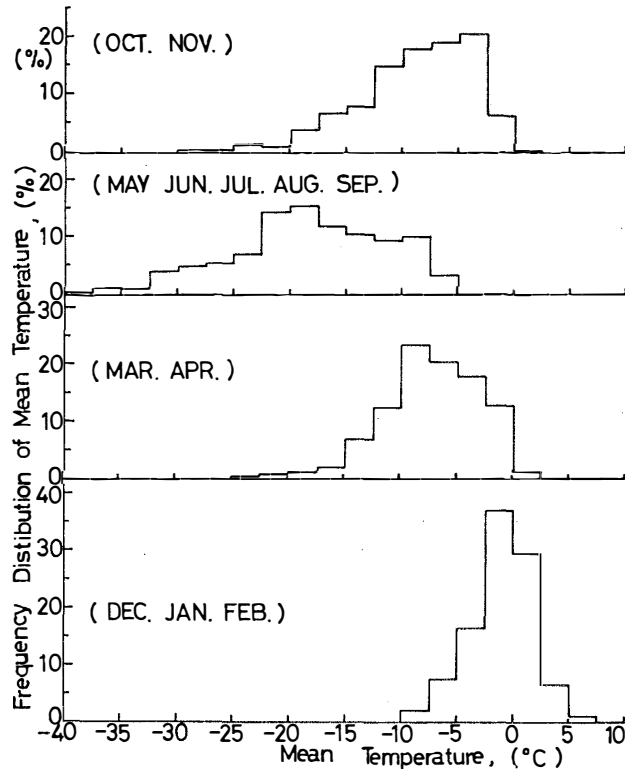


Fig. 25. Frequency distribution of air temperature and its seasonal variation.

(Fig. 23), and almost agree with the starting wind velocity of drifting snow.

3.2.8. Frequency distribution of air temperature (Fig. 25)

In summer, the distribution of air temperature falls mostly in the region between -2.5°C and 2.5°C , and no data below -10°C are obtained. In winter, the range of the frequency distribution is wider than in other seasons, and the maximum distribution is about 15% in the region between -17.5°C and -20°C . On the other hand, the distribution peak in summer is over 35%, in contrast with the distribution pattern of winter-type. The distributions in spring and autumn show a mixed pattern of summer-type and winter-type and show the distribution pattern decreasing gently toward lower temperature regions.

The monthly distribution region is largest in July and smallest in February. The frequency distributions of air temperatures in July 1970 and January 1971 are shown in Fig. 27 (A) as the monthly representative values in winter and summer.

3.2.9. Relation between air temperature and vertical air temperature gradient (Fig. 26)

The relation between the air temperature and the temperature gradient is linear, as the temperature gradient decreases $0.0057^{\circ}\text{C}/\text{m}$ with the 1°C increase of air tem-

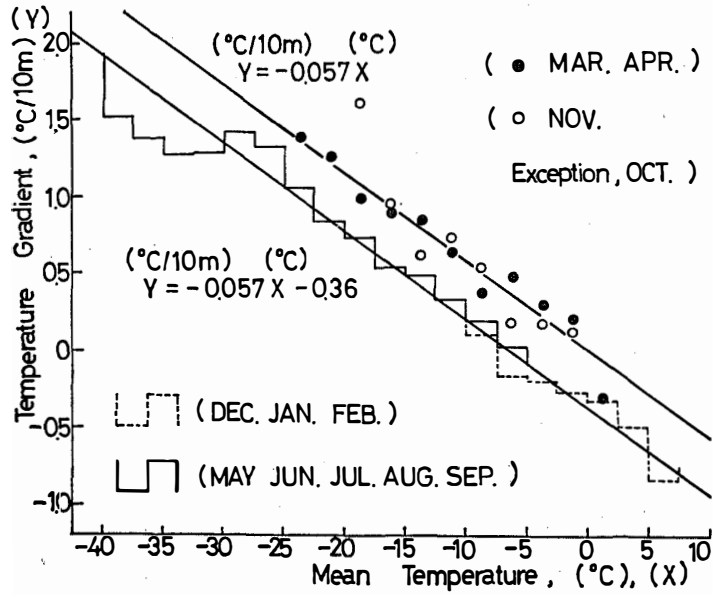


Fig. 26. Relation between the air temperature and the vertical air temperature gradient and its seasonal variation.

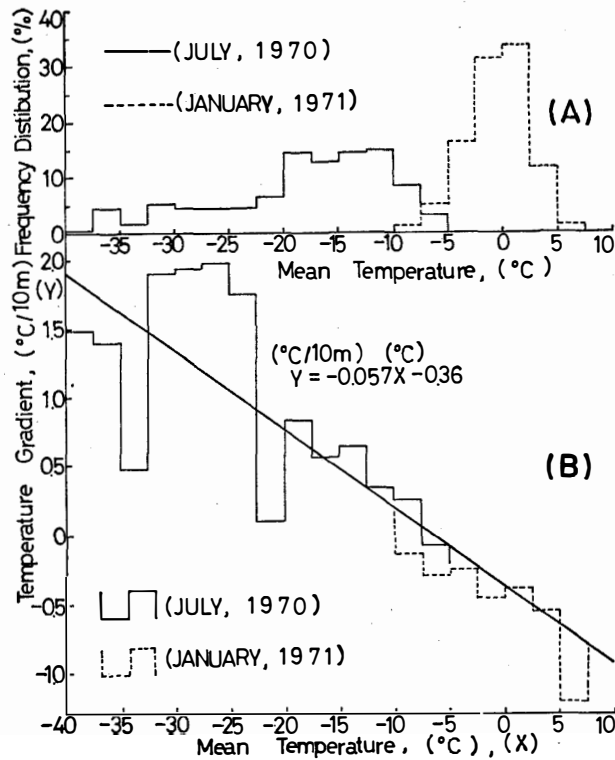


Fig. 27. (A) Frequency distributions of mean air temperatures in July 1970 and January 1971.
 (B) Relations between the air temperature and the vertical air temperature gradient in July 1970 and January 1971.

perature except October. When the air temperature is 0°C , the temperature gradient is $-0.036^{\circ}\text{C}/\text{m}$ in summer and winter and $0^{\circ}\text{C}/\text{m}$ in spring and autumn except October. The abnormal data of October may be explained as that the whole island is covered with snow and ice, so that evaporation and sublimation in daytime and condensation in nighttime are greatly intensified. The relations are represented as follows:

$$\text{Spring and autumn; } Y = -0.0057X,$$

and

$$\text{summer and winter; } Y = -0.0057X - 0.036,$$

where Y is the temperature gradient ($^{\circ}\text{C}/\text{m}$) and X the air temperature ($^{\circ}\text{C}$). And the relations in July 1970 and January 1971 in Fig. 27 (B) are expressed as the same relation mentioned above in summer and winter. Now, the unit of the temperature gradient in Fig. 26 represents the air temperature difference per 10 m ($^{\circ}\text{C}/10\text{ m}$).

3.2.10. Frequency distribution of vertical air temperature gradient (Figs. 28 and 29)

The frequency distribution of the vertical air temperature gradient under stable (positive) conditions is about 88% in winter and about 75% throughout the year on the tower at Syowa Station. The seasonal variation of the frequency distribution is shown in Fig. 28 and the monthly variation of the frequency distribution in Fig. 29.

The variation of the frequency distribution under unstable conditions is about 70% in summer. Even if 30% of the remainder is the stable stability, however, the temperature gradient is almost below 1°C per 10 m. The maxima of the frequency distributions of temperature gradients in July and September are small with about

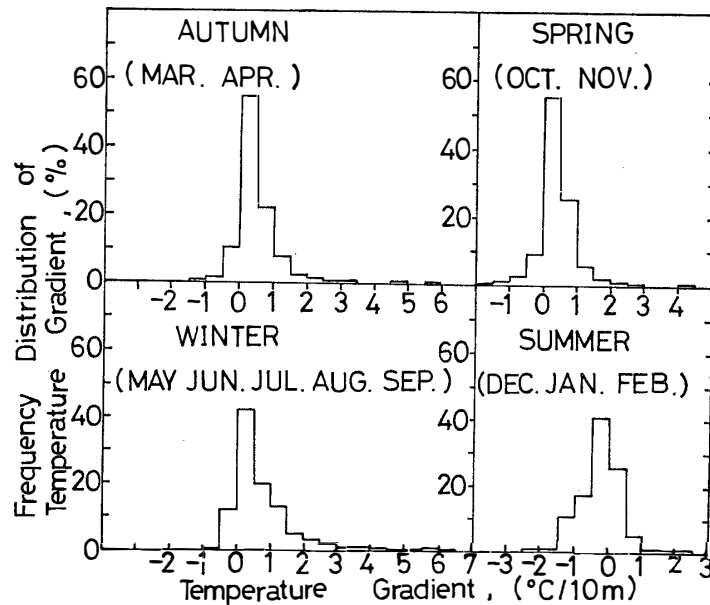


Fig. 28. Seasonal variation of the frequency distribution of vertical air temperature gradient.

30%, on the other hand, they are large in autumn and spring with 53–56%. The frequency distribution patterns of temperature gradients in autumn and spring are similar to those in winter and summer.

The variation pattern of the frequency distribution is nearly symmetric in autumn and spring, but is distorted in other seasons, *i.e.*, the maximum of the frequency distribution in winter shifts from the maximum of the normal distribution to the unstable side, and that in summer to the stable side. The maximum of the frequency distribution is situated within $-0.05-0^{\circ}\text{C}/\text{m}$ in summer and within $0-0.05^{\circ}\text{C}/\text{m}$ in other seasons except September.

SCHWERDTFEGER (1970) reported that the temperature gradient is $1^{\circ}\text{C}/\text{m}$ up to the heights of 20 or 30 m above the snow surface at Plateau Station, the value is represented as the ten-day mean of clear weather (2/10 Ci) in winter. However, the temperature gradient at the observation site of Syowa Station is not much higher than other results.

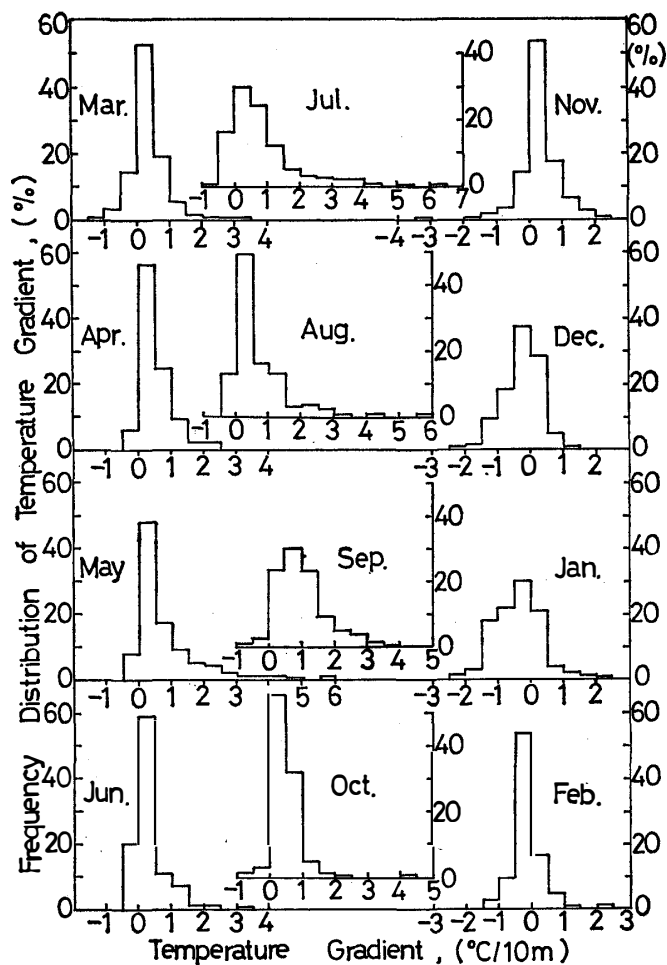


Fig. 29. Monthly variation of the frequency distribution of vertical air temperature gradient.

3.2.11. *Characteristic of meteorological observation at Syowa Station*

The results of July 1970 and January 1971 are selected as the monthly representative values in winter and summer. The monthly variation pattern is more significant in comparison with the seasonal variation. As the monthly variation pattern has been already mentioned above, the results will not be explained here to avoid an overlap.

Each frequency distribution and the interrelations among the wind direction, the wind velocity, the air temperature and the temperature gradient are described. The observation data of wind velocity and temperature gradient are certainly represented as the meteorological data of the limited area at the observation site of Syowa Station, but it is necessary to obtain representative data in a wider region near Syowa Station in Antarctica.

The author observed various meteorological elements above the smooth sea ice of the Ongul Strait about 2 km east of Syowa Station during the period of extreme low temperatures from August 20th to September 19th, 1970. The temperature gradient of $2.0^{\circ}\text{C}/\text{m}$ is obtained as the maximum value of the observation above the sea ice, and the temperature gradient of $1.0^{\circ}\text{C}/\text{m}$ is observed with very high frequency in comparison with the observation on the tower at Syowa Station. It is recognized that the temperature gradient and the wind velocity profile against the height are rather different. As the temperature gradient above the sea ice is obtained from the air temperature of the heights between 4 m and 2 m, the difference may be due to the observation at the low height apparently. However, it is found that the air temperature profile in lower atmospheric surface layer has a nearly linear variation against the height from the snow surface during the period of extreme low temperatures, as shown by LILJEQUIST (1957) and MAKI (1972a). Therefore, the location of the observation site and the topography of the area seem to have greater influence than the difference of temperature gradient against the observation height.

The above results are the measurement values obtained on the tower in the sloping area facing the sea ice on the northeast side of Syowa Station, where the atmosphere is disturbed considerably and the temperature gradient is small. Syowa Station is about 15 m above the sea level and the 21 m-high tower stands at the height of about 8 m above the sea level, so the measurement is subject to the updraft effect of the prevailing, the northeast wind blowing from the sea ice to Syowa Station, and is subject to the spill-over effect of the westward or southward winds blowing from an upper part in East Ongul Island to Syowa Station. In the case mentioned above, the stable stratification tends to be broken.

The wind velocity of the lower atmospheric surface layer becomes relatively strong and the temperature gradient becomes small. Furthermore, characteristics of the wind velocity and air temperature profiles in stable stratification disappear by updraft and spill-over winds caused by the topography of East Ongul Island.

Thus, judging from these results, the observations of the wind velocity and air temperature profiles on this tower do not seem to be ideal as a representative meteorological observation in Antarctica as described by MAKI (1972b). However, the climatic

elements observed at Syowa Station are actual results, it is extremely significant to make a first observation of the air temperature and wind velocity profiles on the tower at Syowa Station in Antarctica in the sence of the necessity of observations of climatic elements.

3.2.12. Occurrence ratio of ground inversion and altitude of ground inversion (Fig. 30)

Figs. 30 (A) and (B) show the annual variation of the monthly mean occurrence ratio of ground inversion (R_x) and the annual variation of the monthly mean altitude of ground inversion (H_x), respectively.

In Fig. 30 (A) the maximum frequency of ground inversion appears in September, and the minimum one in January and February. However, the maximum value of H_x is found in May and June, and H_x is constantly low from spring to summer. In autumn H_x is higher and R_x is relatively smaller. These seasonal variations can be ascribed to the solar radiation which heats up the atmospheric surface layer. The thicker the ground inversion layer, the fewer the occurrence ratio of ground inversion at Syowa Station except in summer.

In Fig. 30 (B), H_x , the thickness of inversion layer is 350–400 m in winter and 250–300 m in summer. If the ground inversion occurs in winter of the temperate zone, e.g., Japan, H_x is nearly equal to the altitude of a thermal belt (Ministry of Agriculture and Forestry, 1961) which shows that the air temperature of the middle

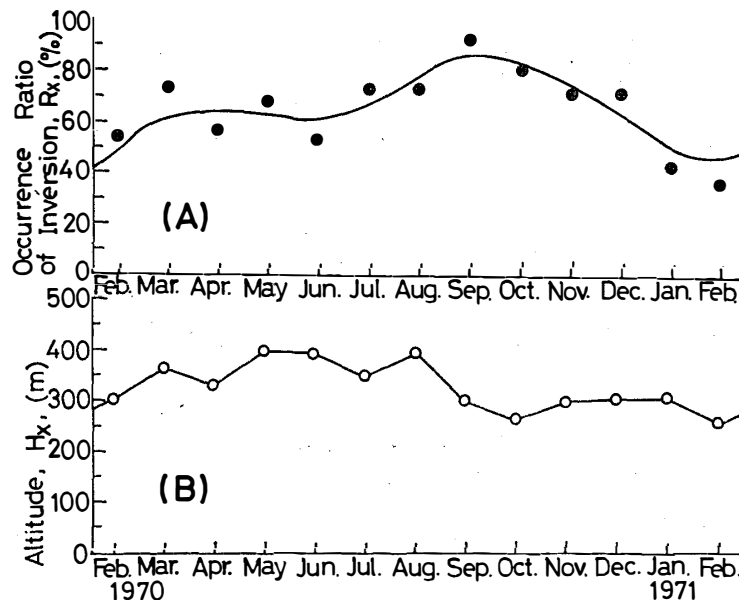


Fig. 30. (A) Annual variation of the monthly mean occurrence ratio of ground inversion at Syowa Station.
 (B) Annual variation of the monthly mean altitude corresponding to the tropospheric maximum air temperature.

high zone of a mountain is higher than that of other zone in the case of ground inversion.

3.2.13. Annual variations of air temperatures and air temperature differences

(Fig. 31)

Fig. 31 (A) shows the annual variations of the air temperatures, T_x , T_{20} and T_1 , obtained under the conditions of ground inversions. These variations are nearly equal to the variation of the mean air temperature by the routine surface observation, e.g., MURAKOSHI (1958) and MURAKOSHI and YATA (1962). However, T_{20} and T_1 in Fig. 31 (A) are lower than the air temperature of the routine surface observation. Since this figure shows the mean air temperature under the condition of ground inversions, the value of T_1 is lower than the mean air temperature at the height of 1 m which

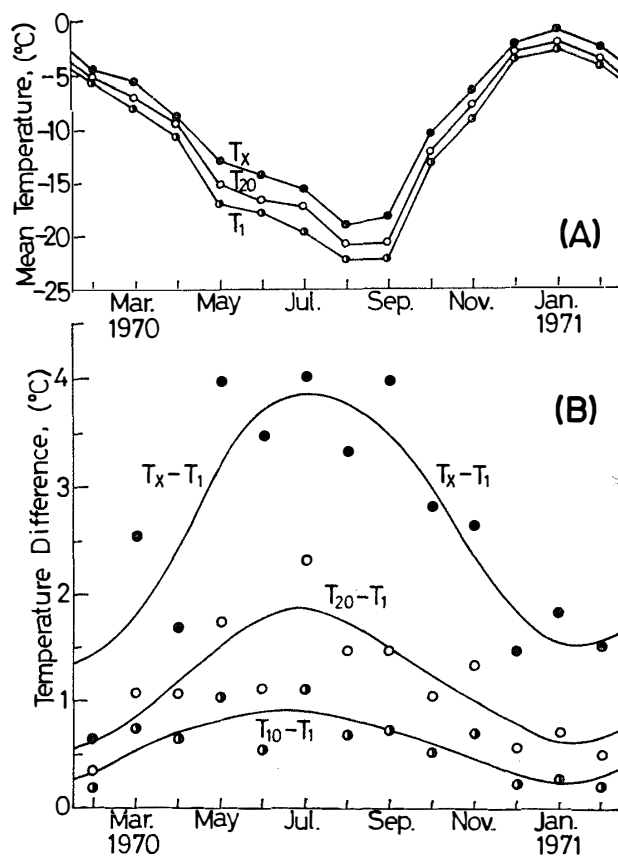


Fig. 31. (A) Annual variations of the monthly mean air temperatures at the altitude corresponding to the tropospheric maximum air temperature (T_x) and at the heights of 20 m and 1 m (T_{20} and T_1) obtained under the condition of ground inversion at Syowa Station. (B) Annual variations of monthly mean air temperature differences $T_x - T_1$, $T_{20} - T_1$ and $T_{10} - T_1$.

is a mean of all cases of the observation. The temperature difference of T_1 is about 1.5°C in winter, about 1.0°C in spring and autumn and about 0.2°C in summer.

As to the tendency of the variation of air temperature, the increase rate of the air temperature which varies from summer to winter is more rapidly than the decrease rate of the air temperature which varies from winter to summer. It is considered intuitively that the air temperature in winter has to fall down continuously, however, in Antarctica the air temperature does not show a sharp fall in full winter, which is the typical variation pattern known as the so-called Kernlose-type (*e.g.*, WEXLER, 1958). This type is also called the pattern of a U-letter type or a pattern of a pan bottom (YAMAZAKI *et al.*, 1969). It is understood that the Kernlose-type pattern is related also to the tropospheric maximum air temperature.

The annual variations of T_x-T_1 , $T_{20}-T_1$ and $T_{10}-T_1$ are shown in Fig. 31 (B). The air temperature difference decreases in the order of T_x-T_1 , $T_{20}-T_1$ and $T_{10}-T_1$. Judging from the difference in the observation heights, this result seems to be natural, because T_x , T_{20} and T_1 are the average values under the condition of ground inversion. The tendencies of the averaged variation of air temperature difference are shown by the solid lines in Fig. 31 (B). It is shown that the variation value is maximum in July and minimum in January and February, *i.e.*, the air temperature difference of ground inversion is large in winter and small in summer.

LILJEQUIST (1957) observed the wind velocity profile, the air temperature profile and the other meteorological elements at Maudheim Station ($71^{\circ}03'S$, $10^{\circ}56'W$) and obtained the frequency distributions of temperature gradient, the tropospheric maximum air temperature (T_x), air temperatures at the heights of 10, 5 and 0 m (T_{10} , T_5 and T_0), air temperature differences of each height and ratios of air temperature differences. It is found that the results at Maudheim Station agree nearly well with the results at Syowa Station for the variation of the frequency distribution of temperature gradient, but the absolute value and the distribution range of temperature gradients at Maudheim Station are 4 times as large as the values at Syowa Station.

The variation tendencies of T_x , T_{10} , T_5 and T_0 and each difference at Maudheim Station agree well with those at Syowa Station. However, each air temperature difference at Maudheim Station is about twice as large as that at Syowa Station. This is because the extremely smooth snow field at Maudheim Station seems to have a stronger effect than the phenomenon which the air temperature is 2.0°C in summer and 5.0°C in winter lower than that at Syowa Station.

3.2.14. Seasonal profiles of air temperatures (Fig. 32)

Fig. 32 shows the characteristic seasonal profiles of air temperatures. The vertical profile of air temperature in winter shows a perfect linear variation and that in spring shows a nearly linear variation. This is because East Ongul Island is mostly covered with snow and ice, and the air temperature is low. The linear profile represents the characteristic of the super-stable stratification in Antarctica.

In autumn, the temperature gradient of the atmospheric surface layer below the height of 10 m is larger than that above the height.

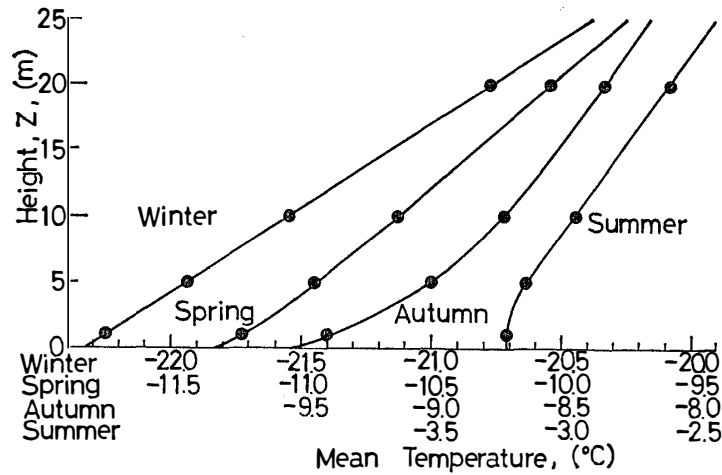


Fig. 32. Seasonal profiles of air temperatures above the sea ice around Syowa Station.

In summer, the temperature gradient of the lower part of the atmospheric surface layer is smaller than in the upper part. Taking into consideration that many cases of unstable stability appear in summer, the characteristic profile mentioned above seems to be naturally understood.

3.3. Observations of atmospheric surface layer, turbulent heat transfer and visibility

3.3.1. Relation between stability ratio and ratio of linear wind velocity component to U_6

Fig. 33 shows the typical wind velocity profile in stable stratification at point B above the sea ice. Fig. 34 shows the relation between the observed values of k and the observed values of S in eq. (19). The plots in Fig. 34 show the intermediate values between maxima and minima of k in the case of stability ratio below 0.10 s^{-2} . The value of k increases rapidly in the case of S below 0.02 s^{-2} and increases gently above 0.02 s^{-2} with the increase of stability ratio. The relation between k and S is expressed by the following equations:

(a) $\log(1/k) = 0.045S^{-0.55}, \dots\dots\dots (20)$

(b) $k = 0.42 \log S + 1.13, \dots\dots\dots (21)$

and

(c) $k = 1/(1 + 0.065S^{-0.79}), \dots\dots\dots (22)$

The observation values agree generally with eqs. (20) and (22). Eq. (21) agrees better with the measurement values $S > 0.005\text{ s}^{-2}$ than eqs. (20) and (22). The mean value of the three equations is mostly coincident with the measurement values. These equations are used to calculate the proportional coefficient of the turbulent heat transfer.

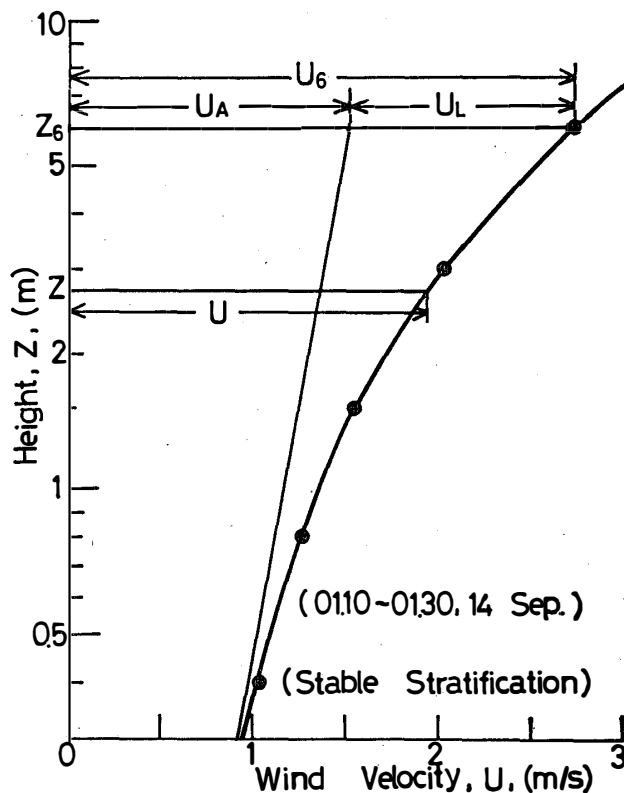


Fig. 33. Typical wind velocity profile in super-stable stratification at point B above the sea ice.

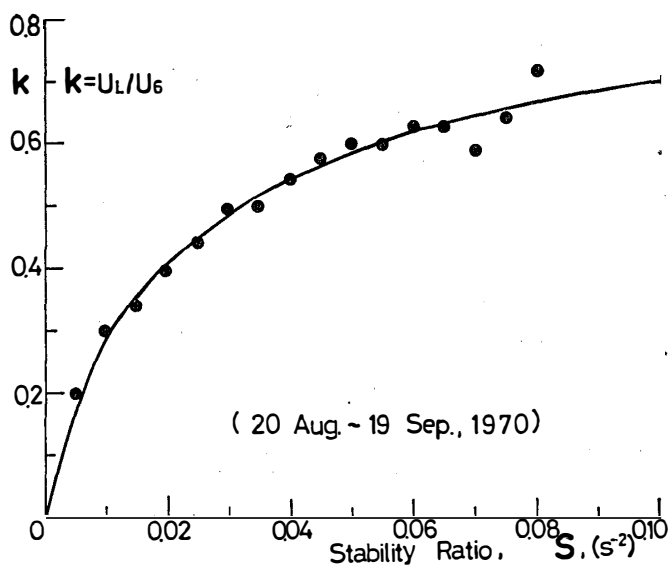


Fig. 34. Relation k and the stability ratio (S). $k (= U_L/U_6)$ is the ratio of the linear component of wind velocity proportional to the height above the snow surface (U_L) to the wind velocity at the height of 6 m (U_6).

Table 4 shows the mean value obtained from the three equations (k_1) and the measurement value (k_2) against the stability ratio (S). The measurement value agrees well with the value obtained from the three equations for $S > 0.001 \text{ s}^{-2}$. The trends of these equations are almost coincident with the results of LILJEQUIST (1957).

Table 4. Relation between k_1 and k_2 against the stability ratio (S). k_1 is the mean value obtained from the three equations and k_2 the measured value.

$S(\text{s}^{-2}) \times 10^{-2}$	0	0.10	0.25	0.50	0.75	1.0	1.5	2.0
$k_1 \times 10^{-2}$	0	3.6	9.2	17.1	23.7	28.7	36.1	41.6
$k_2 \times 10^{-2}$	0	5	10	17	24	29	36	42
$S(\text{s}^{-2}) \times 10^{-2}$	3.0	4.0	5.0	6.0	7.0	8.0	9.0	10.0
$k_1 \times 10^{-2}$	49.3	54.7	58.8	62.0	64.7	67.0	69.0	70.7
$k_2 \times 10^{-2}$	49	55	59	62	65	67	69	71

3.3.2. Variations of momentum diffusion coefficient, mixing length and Richardson number against height

Fig. 35 shows the relation between the height (Z) and the momentum diffusion coefficient (K_M) in eq. (16) against the stability ratio (S). The relation has two asymptotes against each stability ratio. This tendency is like an orthogonal hyperbola. Over the height of few meters in Fig. 35, the value of K_M approaches to an asymptote and is not much different from the discrepancy of height in super-stable stratification.

Fig. 36(A) shows the relation between the height (Z) and the mixing length (l_s)

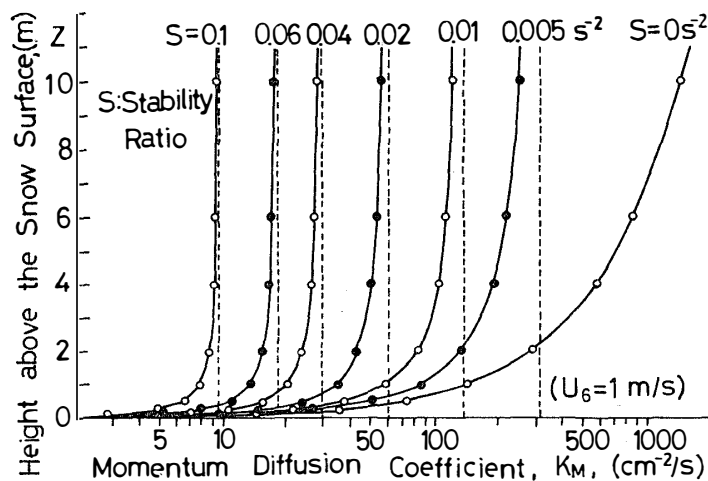


Fig. 35. Relation between the momentum diffusion coefficient (K_M) and the height (Z) against the stability ratio (S) for $U_6 = 1 \text{ m/s}$ in stable stratification.

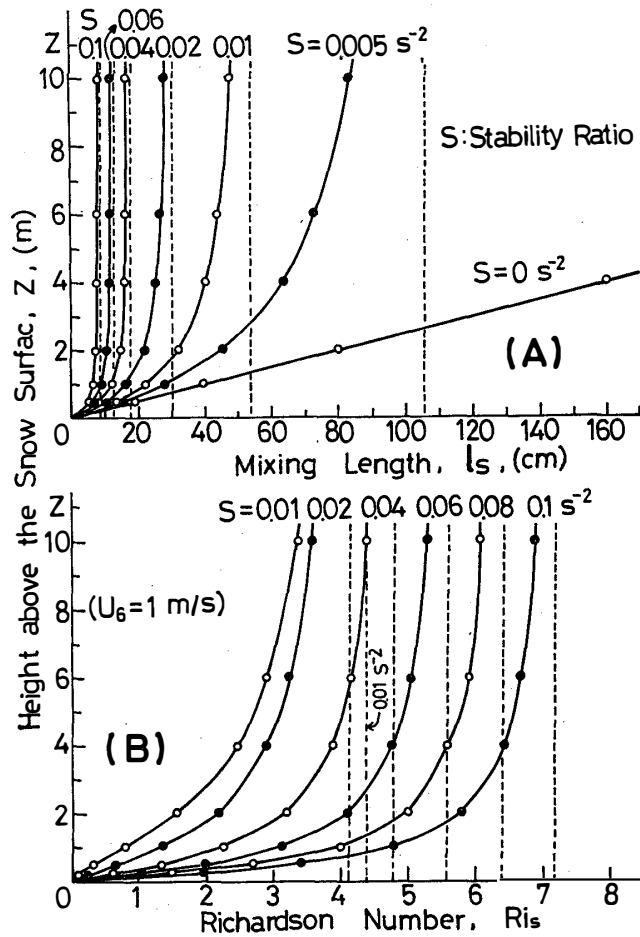


Fig. 36. (A) Relation between the mixing length (l_s) and the height (Z) against the stability ratio (S) in stable stratification. (B) Relation between the Richardson number (Ri_s) and Z against S for $U_6=1$ m/s in stable stratification.

in eq. (17) against the stability ratio (S). In this relation, l_s decreases rapidly with the increase of S . l_s approaches to a constant value with the increase of Z against a constant value of S , i.e., l_s has each asymptote which is parallel to the line of Z against various stability ratios. l_s in neutral stability ($S=0$) is proportional to Z . l_s approaches to zero in super-stable stratification or at the height of zero meter, i.e., l_s , Z and S converge at the zero point respectively.

Fig. 36 (B) shows the relation between the height (Z) and the Richardson number (Ri_s) in eq. (18) against the stability ratio (S) for $U_6=1$ m/s. With the increase of Z against various stability ratios as shown in Fig. 36 (A), Z approaches to constant values of Ri_s , i.e., Ri_s has each asymptote which is parallel to the line of Z against various stability ratios.

An asymptote in nearly neutral stratification is seen to incline toward a higher value of Ri_s . For example an asymptote for $S=0.01$ s⁻² is larger than that for $S=0.02$ s⁻² in the case of the higher observation height. However, the relation is doubtful, as this equation cannot be applied to the relation at the higher observation height. The solid lines are similar to orthogonal hyperbolas except the lower part near snow surface. Ri_s ; Z and S converge at the zero point respectively.

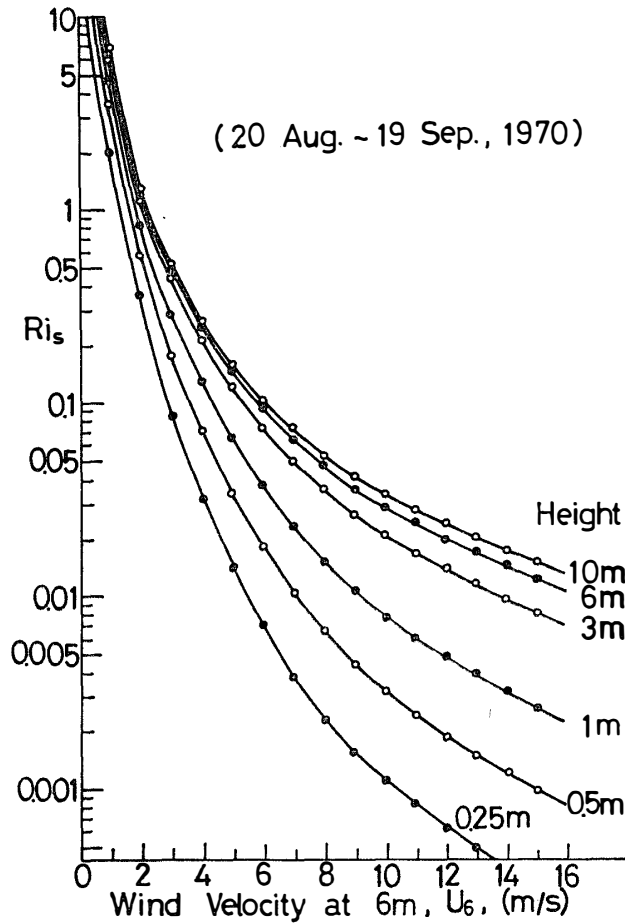


Fig. 37. Relation between the wind velocity at the height of 6 m (U_6) and the Richardson number (Ri_s) against the height (Z) in stable stratification.

Fig. 37 shows the relation between U_6 and Ri_s in eq. (18) against Z . In this relation, Ri_s increases relatively with the increase of Z and with the decrease of U_6 . Ri_s against U_6 decreases rapidly in lower wind velocities and gently in higher wind velocities. The results of K_M , l_s and Ri_s agree with LILJEQUIST's results on the tendency of these equations.

3.3.3. Relation between U_6 and vertical air temperature gradient above the sea ice

The relation between the wind velocity at the height of 6 m (U_6) and the temperature gradient above the sea ice is shown in Fig. 38. The temperature gradient remarkably increases when U_6 is below 5 m/s, and decreases when U_6 is above 8 m/s at which the snow cover begins to drift slightly (MAKI, 1971). The stronger the atmospheric turbulence, the less the temperature gradient. This variation pattern is similar to the pattern in winter (Fig. 23).

To make clear the relation between the wind velocity and the temperature gradient, the observed data are plotted in Fig. 38. From the distribution of the points, the maximum value of the temperature gradient related to the wind velocity

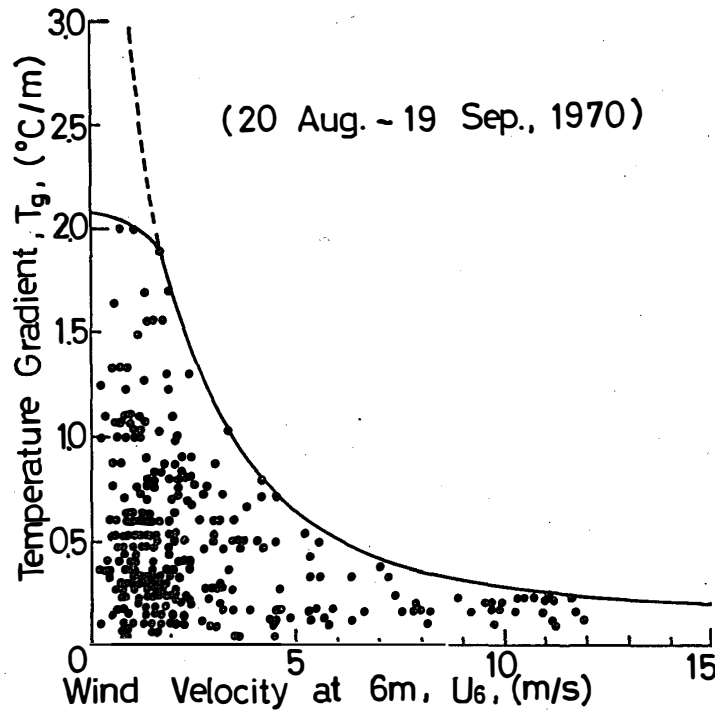


Fig. 38. Relation between the wind velocity at the height of 6 m (U_6) and the vertical air temperature gradient on the sea ice of the Ongul Strait. Solid line indicates the maximum limit of the relation between U_6 and the temperature gradient.

can be estimated. The solid line represents the maximum limit of the relation between the wind velocity and the temperature gradient. The variation pattern of the maximum limit represents approximately an orthogonal hyperbola for $U_6 > 2.0$ m/s, i.e.,

$$T_g = 3.0/U_6,$$

where T_g is the temperature gradient ($^{\circ}\text{C}/\text{m}$) and U_6 the wind velocity at the height of 6 m (m/s). The unit of the proportional coefficient is $^{\circ}\text{C}/\text{s}$.

3.3.4. Relations between wind velocity and aerodynamic roughness length and between wind velocity and friction velocity

Figs. 39 (A) and (B) show the relations between the wind velocities at the heights of 6 m or 20 m (U_6 or U_{20}) and the aerodynamic roughness length (Z_0) and between U_6 or U_{20} and the friction velocity (U_*) calculated from wind velocity profiles for $-0.01 < Ri < 0.05$. At point A, Z_0 has a constant value independently of U_6 as

$$Z_0 = 0.01 \text{ cm}, \dots\dots\dots (23)$$

for $0 < U_6 \leq 13$ m/s and Z_0 is expressed by

$$\log Z_0 = 0.0010 U_6 - 3.30, \dots\dots\dots (24)$$

for $U_6 \geq 13$ m/s, where Z_0 and U_6 are given by the units of cm and cm/s respectively.

The increase of Z_0 under the condition of $U_6 \geq 13$ m/s seems to indicate that the wind energy is consumed in blowing up snow particles, which causes the apparent increase of the roughness of the snow surface with the wind velocity.

On the other hand, at point C the value of Z_0 decreases rapidly from about 3.0 cm to about 0.01 cm with the increase of U_{20} for $U_{20} \leq 15$ m/s. The almost constant variation may be ascribed to the following reason: When the wind, especially the prevailing wind, blows from the direction of the smooth sea ice, the wind velocity influences the updraft effect. It seems that the wind velocity of the lower atmospheric surface layer on the wind velocity profiles is strong as compared with the upper layer.

U_* is shown by the following equation given by eqs. (13) and (23) below 13 m/s of U_6 ,

$$U_* = 0.0365 U_6 \dots \dots \dots (25)$$

The relation between U_6 and U_* is represented by a linear equation below 13 m/s of U_6 . Above 13 m/s of U_6 , however, U_* is shown by

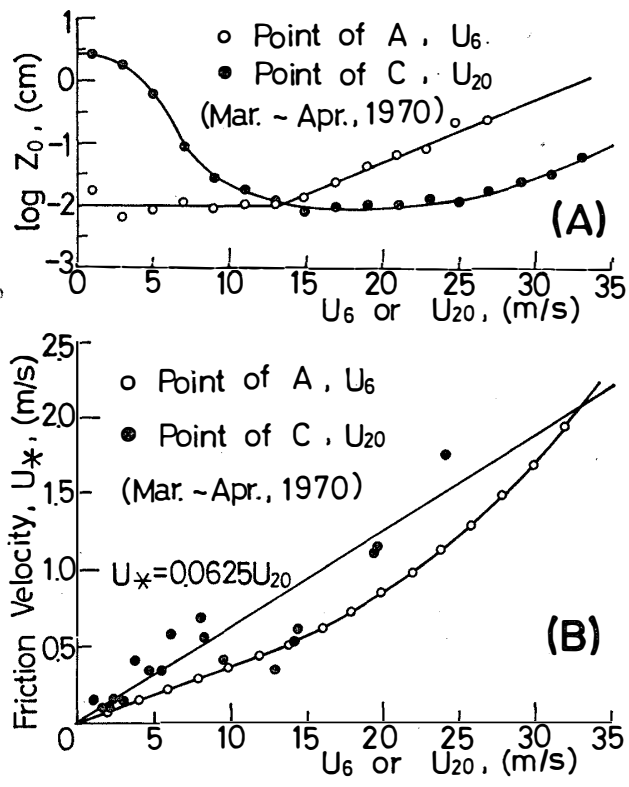


Fig. 39. (A) Relations between the aerodynamic roughness length (Z_0) and the wind velocities at the heights of 6 m or 20 m (U_6 or U_{20}).
 (B) Relations between the friction velocity (U_*) and U_6 or U_{20} .

$$U_* = U_6 / (35.0 - 0.00575U_6), \dots\dots\dots (26)$$

due to eqs. (13) and (24). The relation between U_6 and U_* is represented by an orthogonal hyperbola above 13 m/s of U_6 .

Z_0 increases under the condition of the strong wind velocity over 13 m/s ($U_* > 42.5$ cm/s) above the snow surface. This phenomenon is also found in the case of aerodynamic roughness length with the crop canopy (MAKI *et al.*, 1968; MAKI, 1969; TAKAMI *et al.*, 1969).

In the case of the snow surface, snow particles start to drift slightly over 8 m/s of U_{10} and the density of snow particles increases with the increase of wind velocity (MAKI, 1971). When snow particles are blown up into the air, it is considered that the friction resistance on the snow surface increases, resulting in the increase of aerodynamic roughness length.

The friction velocity (U_*) at the threshold value of drifting snow is 29.1 cm/s at the height of 10 m. If this value of friction velocity is modified to the value of the height of 30 cm, the wind velocity at the height of 0.3 m ($U_{0.3}$) becomes 5 m/s, U_* is 18.2 cm/s and Z_0 is 0.01 cm.

For the sand surface the value of $U_* = 19.6$ cm/s is obtained by NEMOTO *et al.* (1969), when the mean diameter of sand particles is 0.25 mm. The value of Z_0 when sand particles are not blown up is 0.0012 cm. ZINGG (1952) obtained the following values in the wind tunnel; U_* is 30.5 cm/s and Z_0 is 0.031 cm when the mean diameter of sand particles is 0.44 mm.

From these results, it is deduced that the threshold values of drift when the mean diameter of snow particles is 0.02–0.5 mm and that of sand particles 0.25 mm are almost the same as friction velocities (U_*).

3.3.5. Relation between visibility and density of drifting snow

The relation between the visibility and the density of drifting snow is expressed as eq. (27). Assuming that the size of snow particles in drifting snow is uniform or rather the distribution of snow particles is uniform, the relation is shown as follows:

$$\rho_s = k_c / V_s, \dots\dots\dots (27)$$

where ρ_s is the density of drifting snow in the air, V_s the visibility at the height of 1.5 m and k_c the numerical constant (LILJEQUIST, 1957; Editing Committee of Meteorological Handbook, 1959; YAMAZAKI *et al.*, 1969).

The observation results of the relation are shown in Fig. 40. Snow particles start to drift slightly when U_{10} attains to 8 m/s, and V_s decreases rapidly with the increase of U_{10} above 8 m/s, namely, when U_{10} is 15 m/s (U_{10}), V_s is about 150 m; 25 m/s, 10 m; and 35 m/s, 2–3 m.

The changeable pattern in Fig. 40 shows the following relation; if the drifting snow is accompanied by the snowfall and the quantity of snow gains, the solid line is deviated to the left and lower side, whereas if there is no snowfall, the solid line moves to the right and upper side, the dotted lines denote the maximum and minimum values of variations, respectively.

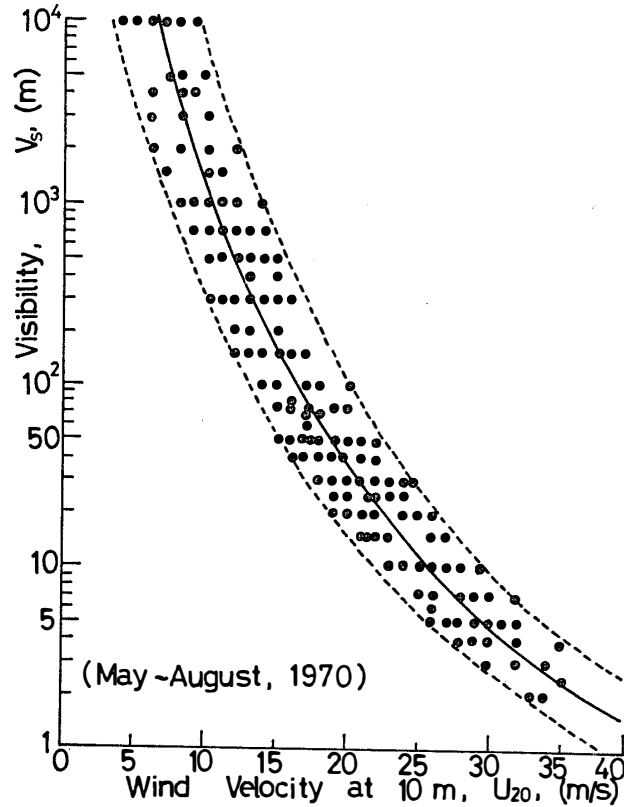


Fig. 40. Solid line is the relation between the visibility at the height of 1.5 m (V_s) and the wind velocity at the height of 10 m (U_{10}). Dotted lines are the maximum and minimum limits of the relation between V_s and U_{10} .

3.3.6. Relation between visibility and friction drag

The friction drag (τ) is generally expressed by

$$\tau = \rho U_*^2, \dots\dots\dots (28)$$

where ρ is the air density and τ is given by eqs. (25) and (28) below 13 m/s of U_6 and by eqs. (26) and (28) above 13 m/s with the increase of U_6 , respectively.

Defining τ_c as the friction drag under constant Z_0 ($=0.01$ cm) with the increase of U_6 up to 35 m/s, the relations between U_6 and τ , between U_6 and τ_c and between U_6 and $\tau - \tau_c$ are shown in Fig. 41. The increasing pattern of τ with the increase of U_6 is the same as τ_c below 13 m/s, but the value of τ_c is smaller than that of τ when U_6 is above 13 m/s, and V_s decreases rapidly. The difference of τ and τ_c is that $\tau - \tau_c$ just shows the momentum (wind energy) consumption to blow up snow particles.

The logarithmic relation between U_{10} and $1/V_s$ from Fig. 40 is shown in Fig. 42 and is represented by

$$\log (1/V_s) = 5.00 \log U_{10} - 8.03. \dots\dots\dots (29)$$

It is found that V_s is in inverse proportion to the 5.0 power of the wind velocity

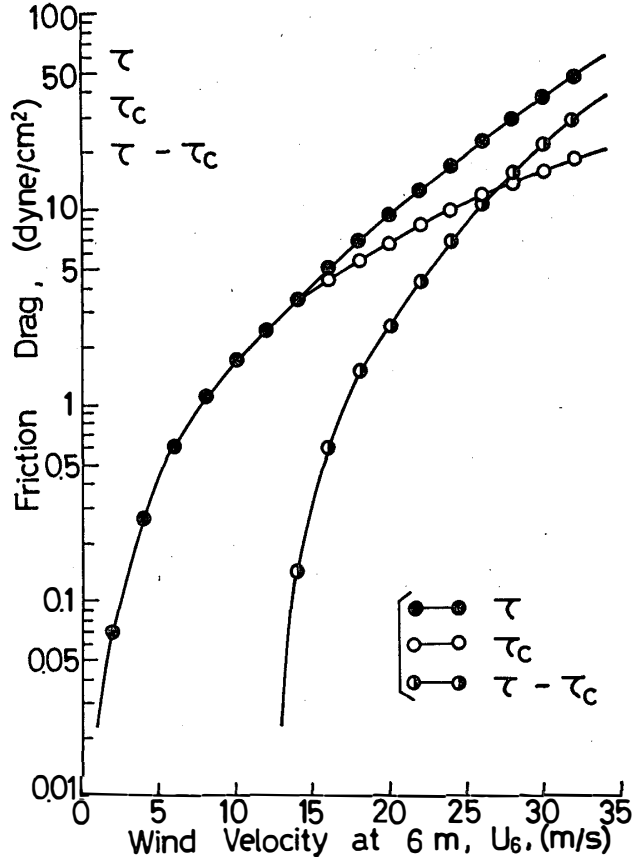


Fig. 41. Relations between τ , τ_c and $\tau - \tau_c$ against the wind velocity at the height of 6 m (U_6). Friction drag (τ) is obtained from the aerodynamic roughness length (Z_0) which is not constant, and the friction drag (τ_c) is obtained from Z_0 which is constant ($=0.01$ cm).

at the height of 10 m (U_{10}) in Fig. 42. The relation between $\tau - \tau_c$ (dyne/cm²) and U_{10} (cm/s) is also shown in this figure, and is expressed as follows:

$$\log(\tau - \tau_c) = 5.10 \log U_{10} - 7.34, \dots \dots \dots (30)$$

It is found that the friction drag is in proportion to the 5.1 power of U_{10} , where the units of V_s , U_{10} and $\tau - \tau_c$ express MKS unit. Furthermore, it is clear that the relation between V_s and $\tau - \tau_c$ is represented by approximately parallel lines in Fig. 42. This result is almost the same as that obtained by LILJEQUIST (1957). The relation between V_s in eq. (29) and $\tau - \tau_c$ in eq. (30) is represented approximately by the following equation:

$$V_s = 5 / (\tau - \tau_c). \dots \dots \dots (31)$$

It is assumed that the units of V_s and $\tau - \tau_c$ are the expression of MKS unit and the unit of the proportional coefficient is m²s²/kg. From eq. (31), it is clear that V_s is in inverse proportion to the difference between τ and τ_c , while τ_c is calculated from

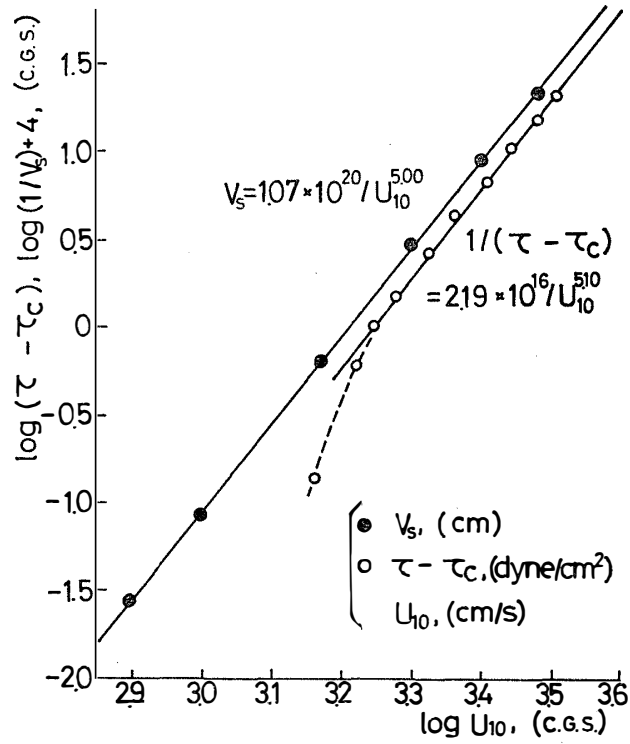


Fig. 42. Logarithmic relation between the difference of friction drag ($\tau - \tau_c$) and the inverse number of the visibility at the height of 1.5 m ($1/V_s$) against the wind velocity at the height of 10 m (U_{10}).

the constant Z_0 and τ is a changeable Z_0 .

Drifting snow particles are blown up from the snow surface by the wind and float in the air in equilibrium with the gravity drifting as fast as the wind velocity. With the increase of snowfall and snow particles blown up from the snow surface and drifting snow particles in the air, V_s is reduced much more. The density of drifting snow in the air increases with the increase of the roughness of the snow surface.

Therefore, when the wind velocity and the friction resistance grow stronger, the drifting snow comes to have a high density and the visibility is reduced. In the valleys, on the contrary, where the wind velocity and the friction resistance are weak, the drifting snow is low in density and the visibility is better. Accumulation of snow particles is largest in the valleys and smallest on the summits where erosion takes place. This phenomenon applies to the rough surface of skavler and the undulation surface in Antarctica.

3.3.7. Sensible heat flux of energy budget equation

We consider the energy budget in winter in Antarctica. If the short-wave radiation

is absent and evaporation or sublimation will be neglected, the energy budget on the snow surface is expressed by a simple equation (Ministry of Agriculture and Forestry, 1961), *i.e.*,

$$Q_e + S_0 + B_0 = 0, \dots\dots\dots (32)$$

where Q_e is the sensible heat flux of the energy budget equation to the snow surface,

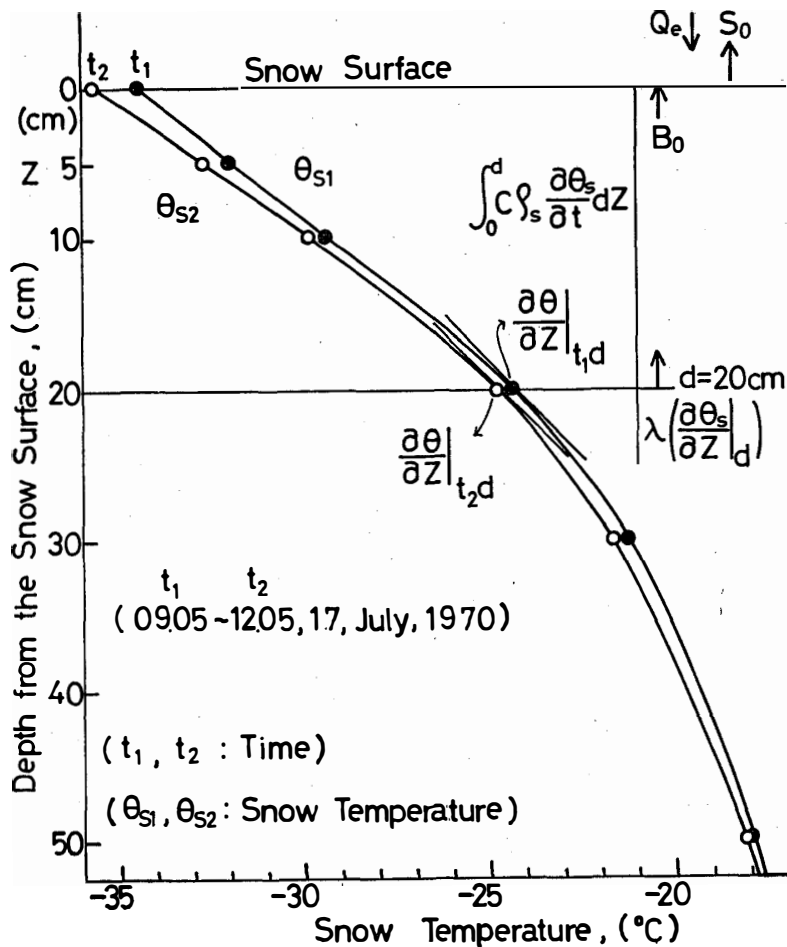


Fig. 13. Energy budget on the snow surface and the typical profiles of the snow temperatures on the sea ice, where Q_e is the sensible heat flux of the energy budget equation to the snow surface, S_0 the net radiation from the snow surface, B_0 the heat flux entering the snow surface from below, d ($=20$ cm) the reference level, $\frac{\partial \theta_s}{\partial Z}|_{t_1 d}$ and $\frac{\partial \theta_s}{\partial Z}|_{t_2 d}$ are the vertical snow temperature gradients at the reference level (d) at t_1 and t_2 , $\int_0^d c_s \rho_s \frac{\partial \theta_s}{\partial t} dz$ is the energy budget of the snow between the snow surface and the depth (d) and $\lambda_s \left(\frac{\partial \theta_s}{\partial Z} \right)_d$ the heat flux entering the depth from below.

S_0 the net long-wave radiation to the snow surface and B_0 the heat conduction flux in the snow to the surface. Furthermore, in spite of the type of energy budget component, the heat entered the snow surface has a positive sign and the heat taken off from the snow surface has a negative sign.

The heat conduction flux in eq. (32) in the snow is represented as follows:

$$B_0 = \lambda_s \left(\frac{\partial \theta_s}{\partial Z} \Big|_d \right) + \int_0^d c_s \rho_s \frac{\partial \theta_s}{\partial t} dZ, \dots \dots \dots (33)$$

where d ($=20$ cm) is the reference depth, c_s the specific heat of the snow, ρ_s the density of the snow, θ_s the snow temperature, t the time, Z the depth and λ_s the heat conductivity. The first component of the right-hand side of eq. (33) shows the heat flux entering the reference level from below and the second component the energy loss of the snow with the unit area situated between the surface and the reference level. The net long-wave radiation (S_0) and the heat conduction flux (B_0) are measured with a net radiometer and L tube thermometers, respectively.

The results obtained at 9.05 and 12.05 on July 17th are given in Fig. 43, exemplifying the typical vertical profiles of snow temperature for the heat conduction flux (B_0).

The specific heat of the snow (c_s) and the density of the snow (ρ_s) are obtained with the snow block, 10 cm cube, which is taken from the snow of the sea ice. The heat conductivity (λ_s) can be obtained by eq. (34):

$$\lambda_s = 0.0036 + 0.426 \rho_s^2. \dots \dots \dots (34)$$

And the thermal conductivity (a^2) is calculated from eq. (35):

$$a^2 = \lambda_s / c_s \rho_s. \dots \dots \dots (35)$$

The following values are obtained:

$$\begin{aligned} c_s &= 0.113 (\text{cal/g} \cdot \text{deg}), \\ \rho_s &= 0.376 (\text{g/cm}^3), \\ \lambda_s &= 6.38 \times 10^{-2} (\text{g} \cdot \text{cal/cm} \cdot \text{min} \cdot \text{deg}), \end{aligned}$$

and

$$a^2 = 2.5 \times 10^{-2} (\text{cm}^2/\text{s}).$$

Now, the snow temperature observation was carried out at intervals of 1–3 hours.

3.3.8. Turbulent heat flux obtained from functional formula including wind component

We consider the turbulent heat flux (Q_w). The radiative diffusivity and the molecular heat conduction are neglected, as they are considerably smaller than Q_w . The heat flux is expressed as follows:

$$Q_w = c_p \rho K_H \frac{\partial \theta}{\partial Z}, \dots \dots \dots (36)$$

where c_p is the air specific heat at a constant pressure, ρ the air density, K_H the heat diffusion coefficient, θ the potential temperature and Z the height.

It is necessary to obtain directly the heat diffusion coefficient (K_H), nevertheless, K_H cannot be obtained accurately and easily in stable stratification. Then Q_w was obtained by the following method: The heat diffusion coefficient (K_H) and the momentum diffusion coefficient (K_M) are assumed as a same coefficient (K) in order to simplify the calculation, i.e., $K_H=K_M=K$. If the air pressure is constant, the relation between the air density and the potential temperature is represented as follows:

$$\rho/\rho_0 = \theta/\theta_0, \dots\dots\dots (37)$$

where ρ_0 and θ_0 are the air density and the potential temperature at 0°C respectively. From eqs. (19), (36) and (37), Q_w is rewritten as follows:

$$Q_w = c_p \rho_0 (\theta_0/g) S K, \dots\dots\dots (38)$$

Then, eq. (38) is substituted with the following numerals for c_p , ρ_0 , θ_0 and g ,

- $c_p = 0.240$ (cal/g·deg),
- $\rho_0 = 1.255 \times 10^{-3}$ (g/cm³),
- $\theta_0 = 273$ (°K),
- $g = 980$ (cm/s²),

and

$$p_a = 982.5 \text{ (mb) (average air pressure during the observation period), i.e.,}$$

$$Q_w = 0.00503 S K, \dots\dots\dots (39)$$

where eq. (39) is expressed as a value per minute. From the values of $U_6 = 1$ m/s and $Z_0 = 0.01$ cm at the height of 6 m shown in Fig. 39 (A), the relation between $K_M = K$,

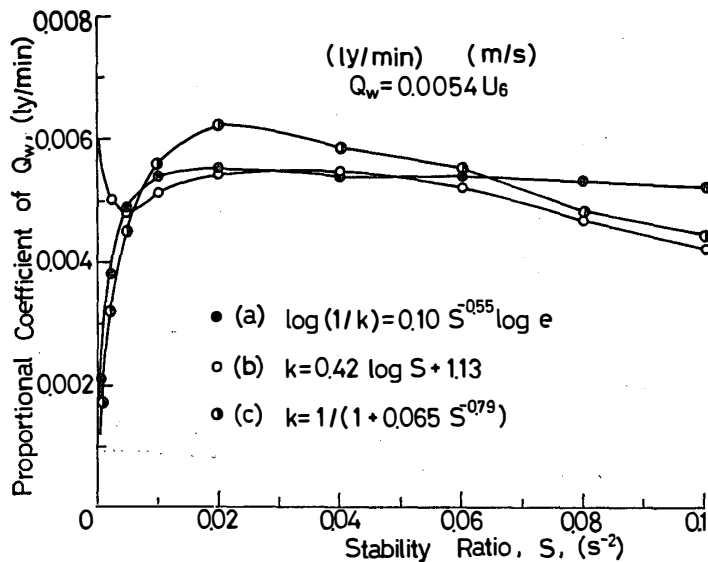


Fig. 44. Relation between the stability ratio (S) and the proportional coefficient of the turbulent heat transfer to the snow surface (Q_w) including the function of k ($=U_L/U_6$) and S , where U_L is the wind component proportional to the height above the snow surface and U_6 the wind velocity at the height of 6 m.

and Z against S is shown in Fig. 35.

K is expressed by the function between k and U_6 , and k is the function of S . After all, Q_w in eq. (30) is substituted with S and U_6 . Fig. 44 shows the relations between the coefficient of Q_w and S , obtained from eqs. (20), (21) and (22) with $U_6=1$ m/s. As the coefficient of Q_w with $Z=6$ m, $U_6=1$ m/s and $Z_0=0.01$ cm is not so changeable for $0.005 < S < 0.1$ s⁻², the mean value of the proportional coefficient of Q_w seems to be represented as a constant value of 0.0054. When U_6 is changeable, eq. (39) is expressed by eq. (40) as a general equation at the height of 6 m,

$$Q_w = 0.0054 U_6 (\text{ly/min}), \dots\dots\dots (40)$$

where U_6 is the unit of m/s.

The relation between Q_e which is obtained from the energy budget and Q_w which is obtained from the wind velocity is shown in Fig. 45. It is naturally obtained that Q_e and Q_w agree considerably.

It is impossible to calculate the sensible heat transfers in August and September, when the sunshine influences the energy budget. As evaporation and sublimation values cannot be estimated, Q_e and Q_w cannot be compared with each other.

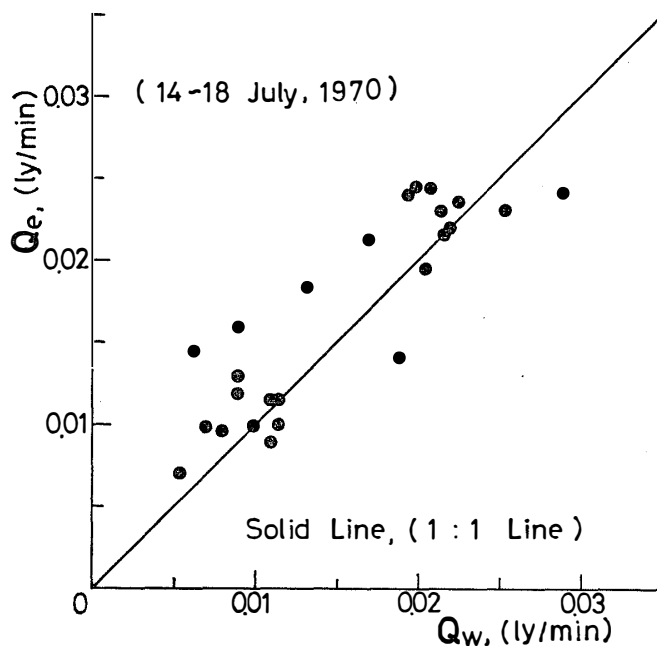


Fig. 45. Relation between the turbulent heat flux obtained from the functional formula including the wind component (Q_w) and the sensible heat flux of the energy budget equation (Q_e).

4. Concluding Remarks

At the slope of about 10-degree inclination, the mean value of the vertical wind speed at the height of 20 m (W_{20}) is about one-third of the longitudinal wind speed at the height of 20 m (U_{20}) and the ratio of W_{20}/U_{20} is independent of Richardson number (Ri) at the height of 20 m. The standard deviations of the longitudinal, lateral and vertical wind speed fluctuations (σ_U , σ_V and σ_W) decrease with the increase of Ri and σ_U/U_{20} , σ_V/U_{20} and σ_W/U_{20} increase exponentially with the increase of Ri . U_{20} decreases exponentially with the increase of Ri at the height of 20 m.

The gustiness decreases exponentially with the increase of U_{20} below about 8.5 m/s of U_{20} and seems to be independent of U_{20} above about 8.5 m/s, and the transition wind speed in Fig. 6(A) may be estimated at about 8.5 m/s at the height of 20 m. The gust factor decreases logarithmically with the increase of U_{20} .

The ratios of σ_U/U_* , σ_V/U_* and σ_W/U_* (U_* is the friction velocity) are almost independent of Ri . The ratios of σ_U/U_* and σ_V/U_* are somewhat smaller and the ratio of σ_W/U_* is somewhat larger than other results because of the topographical effect at the observation site.

The ratio of energy dissipation rate to the third power of U_{20} seems to be proportional to about the 0.5 power of Ri .

Characteristics of frequency distributions of three dimensional wind components under three typical weather conditions were made clear. The maxima of the frequency distribution shift from the mean of the normal distribution to the strong side.

Eulerian auto-correlation coefficients in various stabilities are obtained quantitatively in Fig. 10.

The scales of the largest turbulons of the longitudinal, lateral and vertical wind speeds are independent of Ri . The scale of the atmospheric turbulence is represented by a solid body of a long and narrow cubic vortex having the dimensions of length: breadth : height = 6.3 : 1.9 : 1.

A $-5/3$ power law is applicable to the frequency range above 1.0 c/s or to the nondimensional frequency above 1.0. The nondimensional frequencies at which spectral densities have maximum energy depend on the stability of Ri . With the increase

of Ri , the value of the nondimensional frequency at the maximum spectral density ($u n_p Z / U_{20}$) for the longitudinal wind speed increases exponentially and the value of $w n_p Z / U_{20}$ for the vertical wind speed decreases exponentially. On the other hand, the value of $v n_p Z / U_{20}$ for the lateral wind speed is independent of Ri .

In winter, the frequency of the prevailing wind direction is not higher than that in other seasons, but the frequency of S and SSE wind directions and that of the dead calm (below 0.1 m/s) are higher than those in other seasons.

The mean wind velocity in summer is lower and the prevailing wind velocity in winter is higher than in other seasons.

The air temperatures of the NNE to E wind directions in winter are high and those of SSW and SW low.

The vertical air temperature gradient in stable stratification is larger in the case of ESE to SSW wind directions in winter, and in unstable stratification it is larger in the case of S and SSW in summer. The temperature gradients in winter and summer seem to be symmetric with 0.2°C per 10 m as an axis.

The frequency of the wind velocity below 3 m/s is generally high, being 55.5% in summer and 41.4% in autumn, and that below 1 m/s is high in winter.

The warming ratio of the air temperature with the wind velocity shows a significant annual variation. The ratio is 2.9°C per 10 m/s in spring, 1.3°C in summer, 3.0°C in autumn, 5.0°C in winter, and particularly it is 5.8°C in May and August and 0.5°C in December. The relations by four seasons are given as follows:

$$\begin{aligned} \text{Spring: } Y &= 0.29X - 9.37, \text{ summer; } Y = 0.13X - 1.49, \\ \text{autumn; } Y &= 0.30X - 8.75, \text{ and winter; } Y = 0.50X - 21.29, \end{aligned}$$

where Y is the air temperature (°C) and X the wind velocity (m/s).

In winter, the vertical air temperature gradient in stable stratification decreases rapidly with the increase of the wind velocity below about 10 m/s and gently above 10 m/s. In summer, the temperature gradient in unstable stratification increases rapidly below about 8 m/s, and above 8 m/s the value becomes constant, indicating nearly neutral stratification. The wind velocity of the transition point seems to coincide with the starting wind velocity of drifting snow.

The frequency distribution of air temperature in winter is in contrast with the concentration pattern in summer.

The vertical air temperature gradient decreases 0.0057°C/m with the 1°C increase of air temperature. The relations are represented as follows:

$$\begin{aligned} \text{Spring and autumn; } Y &= -0.0057X, \text{ and} \\ \text{summer and winter; } Y &= -0.0057X - 0.036, \end{aligned}$$

where Y is the temperature gradient (°C/m) and X the air temperature (°C).

The frequency distribution of the air temperature gradient under stable conditions is about 88% in winter, about 30% in summer and about 75% throughout the year. The distribution pattern is nearly symmetric in autumn and spring, but is distorted in other seasons, as the maximum of the frequency distribution shifts from the maximum of the normal distribution to the unstable side in winter and to the stable side in summer.

The monthly variation pattern is more significant than the seasonal variation pattern. The meteorological observations made on the tower built on the sloping terrain of Syowa Station do not seem to be ideal as a representative meteorological observation in Antarctica.

The larger the thickness of inversion layer, the less becomes the occurrence ratio of ground inversion, except in summer.

The Kernlose-type phenomenon occurs in the annual variations of T_x (tropospheric maximum air temperature), T_{20} (air temperature at the height of 20 m) and T_1 (air temperature at the height of 1 m) which are the average values under the conditions of ground inversion. The air temperature difference decreases in the order of $T_x - T_1$, $T_{20} - T_1$ and $T_{10} - T_1$. The maximum value of air temperature difference is recorded in July and the minimum value in January and February.

The vertical profile of air temperature in winter shows a perfect linear variation with the height and that in spring shows a nearly linear variation. The lower part of the air temperature profile has a larger temperature gradient in autumn and has a smaller one in summer.

Three equations are obtained with the relation between the stability ratio (S) and the ratio of the linear component of wind velocity proportional to the height above the snow surface to the wind velocity at the height of 6 m. The mean value of three equations agrees with the measurement value for $S < 0.001 \text{ s}^{-2}$.

The relations between Z and the momentum diffusion coefficient (K_M) against S for $U_6 = 1 \text{ m/s}$, between Z and the mixing length (l_s) against S , between Z and the Richardson number in stable stratification (Ri_s) against S for $U_6 = 1 \text{ m/s}$ and between Ri_s and U_6 against Z are represented in Figs. 35, 36 and 37.

The vertical air temperature gradient remarkably increases below 5 m/s of U_6 and slightly decreases above 8 m/s of U_6 when the snow cover begins to drift. The variation pattern is similar to an orthogonal hyperbola above 2.0 m/s of U_6 .

The aerodynamic roughness length is constant (0.01 cm) below 13 m/s of U_6 and increases with the increase of U_6 above 13 m/s. The friction velocity shows a linear equation below 13 m/s of U_6 and shows an orthogonal hyperbola above 13 m/s.

Snow particles start to drift slightly when U_{10} attains to 8 m/s, and the visibility observed at the height of 1.5 m decreases rapidly with the increase of the wind velocity above 8 m/s, namely, when U_{10} is 15 m/s, the visibility is about 150 m; 25 m/s, 10 m; and 35 m/s, 2–3 m.

The visibility is inversely proportional to the fifth power of the wind velocity. The deduction of different friction drags is almost proportional to the fifth power of the wind velocity, is related to the energy which causes the blowing of snow particles and is almost inversely proportional to the visibility.

The turbulent heat fluxes obtained by two different methods agree considerably, when the sun rises scarcely above the horizon. On the other hand, it is impossible to calculate the sensible heat transfers in August and September, because the sunshine influences considerably the snow surface of the sea ice and the values of evaporation and sublimation are not negligible.

Acknowledgements

The author would like to express his sincere thanks to Dr. E. INOUE, National Institute of Agricultural Sciences, Dr. S. KUBO, ex-director of the Laboratory of Micrometeorology, N. I. A. S., and Mr. Z. SEINO, ex-director of the Antarctic Observation Office, Japan Meteorological Agency, for selecting him to participate in the Eleventh Japanese Antarctic Research Expedition.

The author expresses his thanks to Dr. T. MATSUDA, who was the leader of the 11th JARE, for facilities granted during the whole of the meteorological observation, and Mr. I. ONO, Mr. M. SATOMI and Mr. H. JOBASHI, who were the routine meteorological observation members of the 11th JARE, for their assistance in the observation in Antarctica.

The author is grateful also to Dr. J. KONDO, Tohoku University, and to Dr. K. UEMURA, University of Tokyo, for reading the manuscript and giving constructive criticism, and to Dr. O. YOKOYAMA, National Research Institute for Pollution and Resources, for providing some computer programs.

Numerical calculations were carried out on the electronic computer of HITAC-8000 Series at the Computing Center for Research in the Ministry of Agriculture and Forestry.

References

- BATCHELOR, G. K. (1956) : The Theory of Homogeneous Turbulence, Cambridge Univ. Press, England.
- BERMAN, S. (1965) : Estimating the longitudinal wind spectrum near the ground. *Q. J. R. Met. Soc.*, **91**, 302-317.
- BLACKMAN, R. B. and J. W. TUKEY (1958) : The Measurement of Power Spectra, Dover Publ. Inc., New York.
- BUSCH, N. E., J. A. FRIZZOLA and I. A. SINGER (1968) : The micrometeorology of the turbulent flow field in the atmospheric surface boundary layer. *Acta Polytech. Scand., Physics Including Nucleonics*, **59**, 1-45.
- BUSCH, N. E. and H. A. PANOFSKY (1968) : Recent spectra of atmospheric turbulence. *Q. J. R. Met. Soc.*, **94**, 132-148.
- BUSINGER, J. A., M. MIYAKE, E. INOUE, Y. MITSUTA and T. HANAFUSA (1969) : Sonic anemometer comparison and measurements in the atmospheric surface layer. *J. Met. Soc. Japan*, **47**, 1-12.
- Editing Committee of Meteorological Handbook (1959) : Meteorological Handbook; visibility (in Japanese), Gihodo, Tokyo, 778-780.
- INOUE, E. (1952) : On the structure of wind near the ground (English abstract). *Bull. Natl. Inst. Agric. Sci., Ser. A*, **2**, 1-93.
- INOUE, E., N. TANI and K. IMAI (1955) : Measurements of the wind turbulence over cultivated fields (English abstract). *Bull. Natl. Inst. Agric. Sci., Ser. A*, **4**, 1-36.
- Japan Meteorological Agency (1964) : Surface meteorological data at the Syōwa Base. *Antarct. Met. Data*, **2**, 1-14.
- Japan Meteorological Agency (1971) : Meteorological data at the Syōwa Station in 1970. *Antarct. Met. Data*, **11**, 1-151.
- KAIMAL, J. C. and Y. IZUMI (1965) : Vertical velocity fluctuations in a nocturnal low-level jet. *J. Appl. Met.*, **4**, 576-584.
- KAIMAL, J. C., J. C. WYNGAARD, Y. IZUMI and O. R. COTÉ (1972) : Spectral characteristics of surface-layer turbulence. *Q. J. R. Met. Soc.*, **98**, 563-589.
- KOBAYASHI, S. and T. ISHIDA (1970) : On the wind turbulence during drifting snow (English summary). *Low Temp. Sci., Ser. A*, **28**, 125-133.
- LILJEQUIST, G. H. (1957) : Energy exchange of an antarctic snow-field. *Norw.-Br.-Swed. Antarct. Exped., 1949-52, Sci. Res.*, **II**, Part 1 C and 1 D, 184-298.
- LUMLEY, J. L. and H. A. PANOFSKY (1964) : The Structure of Atmospheric Turbulence, John Wiley & Sons, New York, 99-212.
- MAKI, T., S. TAKAMI and A. SHINJO (1968) : On zero-plane displacement and roughness length in the wind profile over a sorgo canopy (English summary). *J. Agric. Met.*, **24**, 124-132.
- MAKI, T. (1969) : On zero-plane displacement and roughness length in the wind velocity profile equation over a corn canopy (English summary). *J. Agric. Met.*, **25**, 13-18.
- MAKI, T. (1971) : Relationship between the visibility and the wind velocity in drifting snow at Syowa Station (English abstract). *Antarct. Rec.*, **42**, 35-42.
- MAKI, T. (1972a) : The observation of the atmospheric surface layer on the sea ice in Antarctica (English summary). *J. Agric. Met.*, **27**, 137-143.
- MAKI, T. (1972b) : Relations between wind direction, wind velocity, air temperature and temperature gradient at Syowa Station (in Japanese). *Tenki*, **19**, 359-367.
- MAKI, T. (1972c) : The observation of the atmospheric surface layer in stable stratification

- on the sea ice in Antarctica (in Japanese). *Tenki*, **19**, 415-421.
- MAKI, T. (1972d) : On the turbulent heat transfer on the sea ice in Antarctica (English summary). *J. Agri. Met.*, **28**, 89-92.
- MAKI, T. (1974a) : Atmospheric turbulence measurements with the sonic anemometer-thermometer at Syowa Station in Antarctica (English abstract). *Antarct. Rec.*, **48**, 37-51.
- MAKI, T. (1974b) : Characteristics of atmospheric turbulence in stable stratification at Syowa Station in Antarctica. *J. Met. Soc. Japan*, **52**, 32-41.
- MATSUDA, T. (1964) : Microclimate in the community of mosses near Syowa Base at East Ongul Island, Antarctica (English abstract). *Antarct. Rec.*, **21**, 12-24.
- Ministry of Agriculture and Forestry (1961) : Agrometeorological Handbook; heat balance on the soil surface, and small topography and air temperature (in Japanese), Yoken-do, Tokyo, 69-74 and 296-298.
- MITSUTA, Y., M. MIYAKE and Y. KOBORI (1967) : Three dimensional sonic anemometer-thermometer for atmospheric turbulence measurement. WDD Tech. Note, Occas. Rep., Disas. Prev. Res. Inst., Kyoto Univ., 1-20.
- MITSUTA, Y. (1968a) : Application of sonic anemometer-thermometer to the studies of vertical eddy transport processes in the atmospheric boundary layer. Spec. Contrib., Geophys. Inst., Kyoto Univ., **8**, 45-60.
- MITSUTA, Y. (1968b) : Some results of direct measurements of momentum flux in the atmospheric boundary layer by sonic anemometer. *J. Met. Soc. Japan*, **46**, 29-35.
- MITSUTA, Y., T. HANAFUSA and T. MAITANI (1970) : Experimental studies of turbulent transfer processes in the boundary layer over bare soil. *Bull. Disas. Prev. Res. Inst., Kyoto Univ.*, **19-4-167**, 45-58.
- MITSUTA, Y. (1971) : Sonic anemometer-thermometer for atmospheric turbulence measurements. Paper Presented at Symposium on Flow, Its Measurement and Control in Science and Industry, 9-14 May 1971, Pittsburgh, 1-21.
- MIYAKE, M., M. DONELAN and Y. MITSUTA (1970) : Airborne measurement of turbulent fluxes. *J. Geophys. Res.*, **75**, 4506-4518.
- MIYAKE, M. and G. McBEAN (1970) : On the measurement of vertical humidity transport over land. *Boundary-Layer Met.*, **1**, 88-101.
- MIYAKE, M., R. W. STEWART and R. W. BURLING (1970) : Spectra and cospectra of turbulence over water. *Q. J. R. Met. Soc.*, **96**, 138-143.
- MONIN, A. S. and A. M. OBUKHOV (1954) : The basic laws of turbulence mixing in the surface layer of the atmosphere. *Trudy Geofiz. Inst. Akad. Nauk. SSSR*, **24** (151), 163-187.
- MONIN, A. S. (1962) : Empirical data on turbulence in the surface layer of the atmosphere. *J. Geophys. Res.*, **67**, 3103-3109.
- MORITA, Y. (1968) : Winds of katabatic origin observation at Syowa Station (I) (English abstract). *Antarct. Rec.*, **31**, 21-32.
- MURAKOSHI, N. (1958) : Meteorological observations at the Syowa Base during the period from March, 1957 to February, 1958 (English abstract). *Antarct. Rec.*, **4**, 1-22.
- MURAKOSHI, N. and A. YATA (1962) : Meteorological observation at Syowa Base during the 4th Wintering. *Antarct. Rec.*, **15**, 1-11.
- NAKASHIMA, H. (1961) : Statistical investigation of meteorological data at Syowa Base. *Antarct. Rec.*, **11**, 68-74.
- NEMOTO, S., M. MITSUDERA, K. TAKAHASHI, H. UOTSU and S. KOBAYASHI (1969) : On the threshold friction velocity for saltation of sand. *Pap. Met. Geophys.*, **20** (4), 365-383.
- OKAMOTO, M. and E. K. WEBB (1970) : The temperature fluctuations in stable stratification.

- Q. J. R. Met. Soc., **96**, 591-600.
- SAHASHI, K. (1967) : Estimation of evaporation rate by use of a sonic anemometer. Spec. Contrib., Geophys. Inst., Kyoto Univ., **7**, 95-109.
- SCHWERDTFEGGER, W. (1970) : Die Temperaturinversion über dem antarktischen Plateau und die Struktur ihres Windfeldes. Met. Rdsch., **23** (6), 164-171.
- SEINO, Z. and N. SUZUKI (1964) : Description of aerology and seasonal circulation patterns over the Syowa Base in 1961 (English abstract). Antarct. Rec., **23**, 12-31.
- SHIOTANI, M. (1953) : Some notes on the structure of wind in the lower layer of the atmosphere. J. Met. Soc. Japan, **31**, 327-335.
- SHIOTANI, M. (1963) : Some notes on the structures of wind and temperature fields in the lowest air layers. J. Met. Soc. Japan, **41**, 261-269.
- SITARAMAN, V. (1970) : Spectra and cospectra of turbulence in the atmospheric surface layer. Q. J. R. Met. Soc., **96**, 744-749.
- SOMA, S. (1964) : The properties of atmospheric turbulence in high winds (English abstract). J. Met. Soc. Japan, **42**, 372-396.
- SUTTON, O. G. (1953) : Micrometeorology; the Atmosphere in Motion, (2) Turbulent Flow, McGraw Hill, New York, 56-104.
- TAKAMI, S. and T. MAKI (1969) : On the change of plant canopy height with wind velocity (English summary). J. Agric. Met., **25**, 177-181.
- WARNER, J. (1972) : The structure and intensity of turbulence in air over the sea. Q. J. R. Met. Soc., **98**, 175-186.
- WEBB, E. K. (1955) : Autocorrelations and energy spectra of atmospheric turbulence. C.S.I. R. O. Aust. Div. Met. Physics, Tech. Paper, No. 5.
- WEXLER, H. (1959) : Seasonal and other temperature changes in the antarctic atmosphere. Q. J. R. Met. Soc., **85**, 196-208.
- YAMAZAKI, M., R. IBE and H. FUKUTANI (1969) : On the weather and meteorological observation at Syowa Base, Antarctica (in Japanese). Tenki, **16**, 339-348.
- YOKOYAMA, O. (1971) : An experimental study on the structure of turbulence in the lowest 500 meters of the atmosphere and diffusion in it. Rep. Nat. Inst. Poll. Resour., **2**, 1-118.
- ZINGG, A. W. (1952) : Wind tunnel studies of the movement of sedimentary material. Proc. Fifth Hydraulic Conf., 111-135.

*(Manuscript received August 16, 1973;
Revised manuscript received April 18, 1974)*